was supported by a Grant-in-Aid for High Technology Research (HTR) from the Ministry of Education, Science, Sports, and Culture, Japan, by research grants from the Human Science Foundation (HIV-K-14719), by a Grant-in-Aid for AIDS research from the Ministry of Health, Labor, and Welfare, Japan (H17-AIDS-002), and by the Sasakawa Scientific Research Grant from The Japan Science Society. Funding to pay the Open Access publication charges for this article was provided by Ministry of Health, Labor, and Welfare, Japan.

Conflict of interest statement. None declared.

REFERENCES

1. Bridge,A.J., Pebernard,S., Ducraux,A., Nicoulaz,A.L. and Iggo,R. (2003) Induction of an interferon response by RNAi vectors in mammalian cells. *Nat. Genet.*, **34**, 263–264.
2. Sledz,C.A., Holko,M., de Veer,M.J., Silverman,R.H. and Williams,B.R. (2003) Activation of the interferon system by short-interfering RNAs. *Nat. Cell Biol.*, **9**, 834–839.
3. Kariko,K., Bhuyan,P., Capodici,J. and Weissman,D. (2004) Small interfering RNAs mediate sequence-independent gene suppression and induce immune activation by signaling through toll-like receptor 3. *J. Immunol.*, **172**, 6545–6549.
4. Persengiev,S.P., Zhu,X. and Green,M.R. (2004) Nonspecific, concentration-dependent stimulation and repression of mammalian gene expression by small interfering RNAs (siRNAs). *RNA*, **10**, 12–18.
5. Kim,D.H., Longo,M., Han,Y., Lundberg,P., Cantin,E. and Rossi,J.J. (2004) Interferon induction by siRNAs and ssRNAs synthesized by phage polymerase. *Nat. Biotechnol.*, **22**, 321–325.
6. Hornung,V. *et al.* (2006) 5′-triphosphate RNA is the ligand for RIG-I. *Science*, **314**, 994–997.
7. Pichlmair,A., Schulz,O., Tan,C.P., Naslund,T.I., Liljestrom,P., Weber,F. and Reis e Sousa,C. (2006) RIG-I-mediated antiviral responses to single-stranded RNA bearing 5′-phosphates. *Science*, **314**, 997–1001.
8. Marques,J.T., Devosse,T., Wang,D., Zamanian-Daryoush,M., Serbinowski,P., Hartmann,R., Fujita,T., Behlke,M.A. and Williams,B.R. (2006) A structural basis for discriminating between self and nonself double-stranded RNAs in mammalian cells. *Nat. Biotechnol.*, **24**, 559–565.
9. Sakai,A., Hirabayashi,Y., Aizawa,S., Tanaka,M., Ida,S. and Oka,S. (1994) Investigation of a new p24 antigen detection system by the chemiluminescence-enzyme-immuno-assay. *J. Jpn. Assoc. Infect. Dis.*, **73**, 205–212.
10. Hamazaki,H., Ujino,S., Miyano-Kurosaki,N., Shimotohno,K. and Takaku,H. (2006) Inhibition of hepatitis C virus RNA replication by short hairpin RNA synthesized by T7 RNA polymerase in hepatitis C virus subgenomic replicons. *Biochem. Biophys. Res. Commun.*, **343**, 988–994.
11. Cory,A.H., Owen,T.C., Barltrop,J.A. and Cory,J.G. (1991) Use of an aqueous soluble tetrazolium/formazan assay for cell growth assays in culture. *Cancer Commun.*, **3**, 207–212.
12. Sohail,M., Doran,G., Riedemann,J., Macaulay,V. and Southern,E.M. (2003) A simple and cost-effective method for producing small interfering RNAs with high efficacy. *Nucleic Acids Res.*, **31**, e38.
13. Donze,O. and Picard,D. (2002) RNA interference in mammalian cells using siRNAs synthesized with T7 RNA polymerase. *Nucleic Acids Res.*, **30**, e46.
14. Samuel,C.E. (2001) Antiviral actions of interferons. *Clin. Microbiol. Rev.*, **14**, 778–809.
15. Paillart,J.C., Shehu-Xhilaga,M., Marquet,R. and Mak,J. (2004) Dimerization of retroviral RNA genomes: an inseparable pair. *Nat. Rev. Microbiol.*, **2**, 461–472.
16. Jakobsen,M.R., Damgaard,C.K., Andersen,E.S., Podhajska,A. and Kjems,J (2004) A genomic selection strategy to identify accessible and dimerization blocking targets in the 5′-UTR of HIV-1 RNA. *Nucleic Acids Res.*, **32**, e67.
17. Laughrea,M., Jette,L., Mak,J., Kleiman,L., Liang,C. and Wainberg,M.A. (1997) Mutations in the kissing-loop hairpin of human immunodeficiency virus type 1 reduce viral infectivity as well as genomic RNA packaging and dimerization. *J. Virol.*, **71**, 3397–3406.
18. St. Louis,D., Gotte,D., Sanders-Buell,E., Ritchey,D.W., Salminen,M.O., Carr,J.K. and McCutchan,F.E. (1998) Infectious molecular clones with the nonhomologous dimer initiation sequences found in different subtypes of human immunodeficiency virus type 1 can recombine and initiate a spreading infection in vitro. *J. Virol.*, **72**, 3991–3998.
19. Skripkin,E., Paillart,J.C., Marquet,R., Ehresmann,B. and Ehresmann,C. (1994) Identification of the primary site of the human immunodeficiency virus type 1 RNA dimerization in vitro. *Proc. Natl. Acad. Sci. USA*, **91**, 4945–4949.
20. Shen,N., Jette,L., Liang,C., Wainberg,M.A. and Laughrea,M. (2000) Impact of human immunodeficiency virus type 1 RNA dimerization on viral infectivity and of stem-loop B on RNA dimerization and reverse transcription and dissociation of dimerization from packaging. *J. Virol.*, **74**, 5729–5735.
21. McBride,M.S. and Panganiban,A.T. (1996) The human immunodeficiency virus type 1 encapsidation site is a multipartite RNA element composed of functional hairpin structures,. *J. Virol.*, **70**, 2963–2973.
22. Paillart,J.-C., Berthoux,L., Ottmann,M., Darlix,J.L., Marquet,R., Ehresmann,B. and Ehresmann,C. (1996) A dual role of the putative RNA dimerization initiation site of human immunodeficiency virus type 1 in genomic RNA packaging and proviral DNA synthesis. *J. Virol.*, **70**, 8348–8354.
23. Clever,J.L. and Parslow,T.G. (1997) Mutant human immunodeficiency virus type 1 genomes with defects in RNA dimerization or encapsidation. *J. Virol.*, **71**, 3407–3414.
24. Berkhout,B. and van Wamel,J.L. (1996) Role of the DIS hairpin in replication of human immunodeficiency virus type 1. *J. Virol.*, **70**, 6723–6732.
25. Skripkin,E., Paillart,J.C., Marquet,R., Blumenfeld,M., Ehresmann,B. and Ehresmann,C. (1996) Mechanisms of inhibition of in vitro dimerization of HIV type 1 by sense and antisense oligonucleotides. *J. Biol. Chem.*, **271**, 28812–28817.
26. Lodmell,J.S., Paillart,J.C., Mignot,D., Ehresmann,B., Ehresmann,C. and Marquet,R. (1998) Oligonucleotide-mediated inhibition of genomic RNA dimerization of HIV-1 strains MAL and LAI: a comparative analysis. *Antisense Nucleic Acid Drug Dev.*, **8**, 517–529.
27. Akkina,R.K., Walton,R.M., Chen,M.L., Li,Q.X., Planelles,V. and Chen,I.S. (1996) High-efficiency gene transfer into $CD34^+$ cells with a human immunodeficiency virus type 1-based retroviral vector pseudotyped with vesicular stomatitis virus envelope glycoprotein G. *J. Virol.*, **70**, 2581–2585.
28. Lin,R., Genin,P., Mamane,Y. and Hiscott,J. (2000) Selective DNA binding and association with the CREB binding protein coactivator contribute to differential activation of alpha/beta interferon genes by interferon regulatory factors 3 and 7. *Mol. Cell. Biol.*, **20**, 6342–6353.

J. Biochem. **143**, 339–347 (2008)
doi:10.1093/jb/mvm225

Recognition of a Bulged RNA by Peptides Derived from the Influenza NS1 Protein

Tatsuhiko Someya*,†, Kazumi Hosono†, Kaori Morimura, Hiroshi Takaku and Gota Kawai‡

Department of Life and Environmental Sciences, Faculty of Engineering, Chiba Institute of Technology, 2-17-1 Tsudanuma, Narashino-shi, Chiba 275-0016, Japan

Received August 27, 2007; accepted November 12, 2007; published online November 26, 2007

A competition assay for RNA binding by the influenza virus NS1 protein using model RNAs, U6–45, corresponding to U6 snRNA revealed that deletion of each of the three bulged-out parts reduced the NS1 protein binding and, in contrast, by deleting all three of the bulged-out parts, simultaneously, and thus producing a double-stranded RNA, the binding was recovered. A common feature of target RNAs of the NS1 protein, U6 snRNA, poly(A) and viral RNA, is the stretch of 'bulged-out' A residues. Thus, the NS1 protein was found to recognize either the stretch of 'bulged-out' A residues or dsRNA which is also a target of the NS1 protein. Furthermore, a basic peptide, NS1–2, derived from the helix-2 of the RNA binding site of NS1 protein was designed and its binding to the U6 snRNA was analysed by using a model RNA for U6 snRNA, U6–34. The NMR signals due to H8/H6 and H1′ of U6–34 were assigned and their changes upon binding of NS1–2 were analysed. It was indicated that NS1–2 interacts with the residues in the bulge-out region of U6–34. These results suggest that NS1–2 recognizes the U6 snRNA in a similar manner to NS1 protein.

Key words: gel shift, influenza virus, NMR, NS1 protein, RNA-binding protein, U6 snRNA.

Abbreviations: dsRNA, double-stranded RNA; PAGE, polyacrylamide gel electrophoresis; NS1, non-structural protein 1; snRNA, small nuclear RNA.

Non-structural protein 1 (NS1) of influenza virus type A, consisting of 202–237 amino acid residues, is encoded on the smallest segment, the eighth segment, and forms a homo-dimer (*1–5*). The NS1 protein consists of at least two functional domains: the RNA-binding domain, located on the N-terminal half, and the effector domain (*6*). Between the two domains, an eIF4GI-binding domain was also found (*7*). The NS1 protein affects several steps of host translation, including the inhibition of nuclear export of mature cellular mRNA by binding to the 3′ poly(A) tail (*8*), and the inhibition of mRNA splicing by binding to the U6 snRNA and U6atac snRNA (*9–11*). The NS1 protein also binds to double-stranded RNA (dsRNA) (*12, 13*), which inhibits the antiviral activity of the IFN-α/β-induced 2′-5′-oligo(A) synthetase/RNase L pathway (*14*). Furthermore, the NS1 protein binds to viral RNAs (*15–17*) and increases their translation level in combination with binding to eIF4GI (*7*). Thus, NS1 protein binding to different kinds of RNA with various sequences and structures is important for its function.

The solution and crystal structures of an RNA binding domain of NS1 protein, NS1(1–73), have been reported (*18, 19*). The NS1(1–73) consists of the amino acid residues 1–73 of the NS1 protein, and forms a dimer with the same RNA-binding activity as the full-length protein (*5*). The NS1(1–73) protein monomer was found to consist of three α-helices, with no β-sheets (Fig. 1A). U6 snRNA is one of the members of small nuclear RNAs, and interacts with U2 and U4 snRNA during the pre-mRNA splicing reaction (for review, see *20*).

Mutagenesis experiments suggested that RNA binding requires the dimer formation and the arginine residue at position 38 and the lysine residue at position 41, both of which are located in the second helix of each monomer, are the only amino acid residues that are absolutely required only for RNA binding, but not for the dimerization (*18*). However, the mechanism of the binding of NS1 protein to its RNA targets is still not known.

Figure 2A shows the secondary structure of human U6 snRNA (*21, 22*). The NS1 protein-binding site was reported to be in the range of residues 37–43 and 88–95 including the 5 bulge-out residues by Qin, Y. *et al.* (*10*). This region was shown to include a stem structure by Harada *et al* (*21*) as shown in Fig. 2A whereas Rinke *et al.* (*22*) showed that the region forms an internal loop structure.

In the present study, to analyse the RNA binding properties of the NS1 protein, the affinity of its RNA binding domain to model RNAs, U6–45 corresponding to the U6 snRNA (Fig. 2B), was analysed by a competitive gel shift assay *in vitro*. Our results indicate that the NS1 protein recognizes either the stretch of 'bulged-out' A residues or dsRNA. Furthermore, we also designed two

*Present address: Graduate School of Life and Environmental Sciences, University of Tsukuba, 1-1-1 Tennodai, Tsukuba-shi, Ibaraki 305-8572, Japan.
†These authors contribute to this work equally.
‡To whom correspondence should be addressed. Fax: +81-47-478-0425, E-mail: gkawai@sea.it-chiba.ac.jp

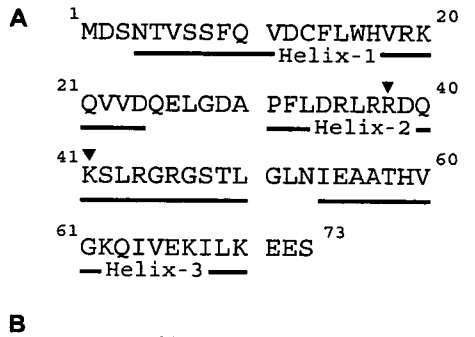

Fig. 1. **Amino acid sequence of a protein and peptides used in this study.** Amino acid sequence of the RNA binding domain of NS1 protein is shown with the position of the three α-helices indicated by underlines (A). Residues involved in direct RNA binding, Arg38 and Lys41, are indicated by arrowheads (*26*). The mutant peptides were derived from the helices-2 and -3 of the RNA-binding domain and three hydrophobic residues are replaced by alanine, indicated by italic font, for each peptide (B).

peptides derived from NS1 protein; NS1–2 and NS1–3 correspond to the helices -2 and -3, respectively (Fig. 1B). For each peptide, some hydrophobic residues are replaced by alanine residues to increase the water solubility. The gel shift assay using these peptides and a shorter model RNA, U6–34 (Fig. 2C) indicated that the short peptide NS1–2 possesses the RNA binding activity. It was confirmed by NMR experiments that NS1–2 binds to the bulge-out region of U6–34.

MATERIALS AND METHODS

Preparation of the Influenza NS1 Protein and Related Peptides—The influenza NS1 protein (A/PR/8/34 strain) was overproduced and fractionated essentially as described by Young *et al.* (*23*), except that the host strain for the expression plasmid pAS-NS (a gift from Dr S. Nakata) was *Escherichia coli* strain N4830-1 (Amersham Pharmacia Biotech). We added an extra purification step, involving anion-exchange column chromatography, with a linear gradient of 50–200 mM NaCl in 40 mM Tris–HCl (pH 8.0). The purity of NS1 protein was analysed by 15% SDS–PAGE using Coomassie Brilliant Blue staining. Peptide samples were purchased from Sawady Technoloty Co. Ltd.

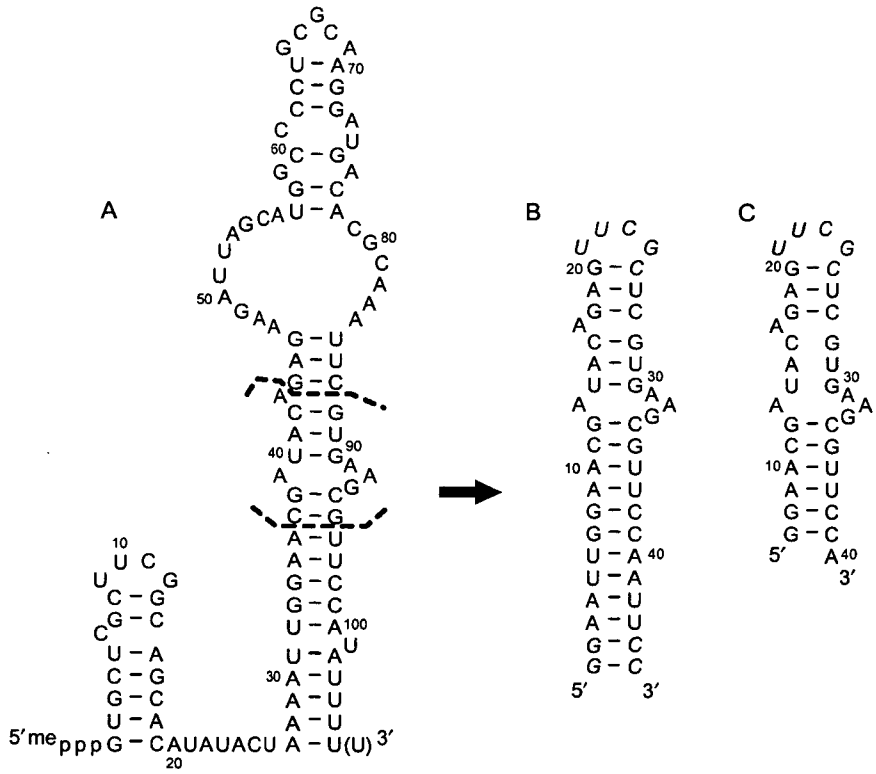

Fig. 2. **Secondary structures of human U6 snRNA (A) and model RNAs, U6–45 (B), and U6–34 (C).** The NS1 binding site of human U6 snRNA is indicated by broken lines according to Qin *et al.* (*10*). U6–45 was designed to include the NS1 binding site. The two strands were connected with the stable UUCG loop, and the terminal base pairs were changed to GC pairs to increase the production yield for *in vitro* transcription by using the T7 RNA polymerase. A model RNA, U6–34, includes the NS1 protein binding site (C). Two strands were also connected with the stable UUCG loop, and the GU base pair closing the UUCG loop was changed to a GC pair. These modifications are indicated by italic font. The residue number is defined for U6–45, which does not correspond to that of U6 snRNA for convenience. The secondary structure of U6–34 reflected the result of the present NMR analysis.

Preparation of RNA Samples—5′-fluorescein-labelled U6–45 RNAs were chemically synthesized with a DNA/RNA synthesizer (Expedite 8909, Perseptive) using fluorescein phosphoramidite (Glen Research). After deprotection, the 5′-fluorescein-labelled RNAs were purified using 20% polyacrylamide gel electrophoresis (PAGE) under denaturing conditions with 8 M urea, and extensively desalted by ultrafiltration. Non-labelled U6–45 and its mutant RNAs were also synthesized by the same method.

For NMR measurements, U6–34 RNAs were enzymatically synthesized by an *in vitro* transcription reaction using T7 RNA polymerase. To improve the resolution of NMR signals, semi-selective [^{13}C, ^{15}N] labelling was introduced to A/U, A, G and C using [*U*-^{13}C,^{15}N]NTPs (Taiyo Nippon Sanso). The transcripts were purified by 15% PAGE under denaturing conditions with 7 M urea, and extensively desalted by ultrafiltration.

For purified RNA samples were annealed by heating at 95°C for 5 min and snap-cooling on ice. The formation of the hairpin structure for each RNA sample was confirmed by PAGE under native condition.

RNase Probing Analyses—For the RNA digestion reaction, 5′-fluorescein-labelled RNA (0.1 μM) was used. RNA samples were dissolved in 20 mM Tris–HCl (pH 7.8), 5 mM $MgCl_2$, 100 mM NaCl and 1 mM dithiothreitol. The reactions were carried out on ice for 5–15 min in the presence of 1, 6 and 0.02 units of RNase T_1, T_2 and V_1, respectively. The digests were analysed by 20% PAGE with an acrylamide:bis ratio of 19:1, in 80 mM Tris–borate (pH 8.3), 2 mM EDTA and 8 M urea, and a plate size of 200 × 400 mm. Detection and analysis of RNAs were performed using the gel analysis system, FLA-2000G (Fuji Photo Film Co., Ltd).

Competitive Gel Shift Assay—The 5′-fluorescein-labelled RNA was mixed with the NS1 protein in the presence of various concentration of non-labelled RNA, and the formation of a labelled RNA-NS1 protein complex was analysed by PAGE under the native condition. Prior to PAGE analysis, samples were mixed in binding buffer containing 5 mM Tris–HCl (pH 7.8), 50 mM KCl, 8% glycerol and 1 mM dithiothreitol, and were incubated at 4°C for 30 min. The sample concentrations in the binding buffer were 0.05 μM for labelled RNA, 0.12 μM for the NS1 protein as the monomer and 0–1 μM for non-labelled RNA. The NS1-protein bound RNAs were separated from the unbound RNA by 6% PAGE with acrylamide:bis ratio of 59:1, in 20 mM Tris–borate (pH 8.3), 0.5 mM EDTA and a plate size of 100 × 100 mm. The relative amounts of free and bound RNAs were determined by using the gel analysis system FLA-2000G.

Gel Shift Assay for Peptides—Prior to gel shift assay with PAGE, samples were mixed in a binding buffer containing 30 mM sodium phosphate buffer (pH 6.9) and 50 mM NaCl, and incubated at 4°C for 30 min. Concentrations of the samples in the binding buffer were 0.05 mM for the RNA and 0–1 mM for each peptide. The peptide-bound RNA was separated from free RNA by 10% PAGE with a condition of acrylamide:bis = 19:1, 45 mM Tris–borate (pH 8.3), 1 mM EDTA. The electrophoresis was performed for 90 min at 100 V/cm with a plate of 100 × 100 mm under the ambient temperature of 4°C. After the electrophoresis, the gels were stained with Toluidinblau O (Chroma Gesellschaft Schmidt & Co.) to visualize RNA containing bands.

NMR Measurements—RNA samples in 30 mM sodium phosphate buffer (pH 6.9) containing 50 mM NaCl were concentrated to 0.1–0.9 mM by ultrafiltration. Peptide samples were dissolved in 30 mM sodium phosphate buffer (pH 6.9) containing 50 mM NaCl. NMR spectra were recorded on a DRX-500 or DRX-600 spectrometer (Bruker) at probe temperatures of 22–32°C. Signals of the exchangeable protons were assigned by using the 2D NOESY spectrum measured in H_2O with a mixing time of 250 ms using the jump-and-return scheme. Signals of non-exchangeable protons were assigned by using the 2D NOESY and 2D TOCSY spectra with mixing times of 300 and 50 ms, respectively. 2D HCCH-COSY and 2D HCCH-TOCSY spectra of the labelled samples were used to assign sugar spin systems (*24*). H2 protons of adenosine were assigned using the 2D HCCH-TOCSY and 2D HSQC spectra of the labelled sample (*25*).

RESULTS

Design of the Model RNAs and RNA Digestion Analyses—According to the results of Qin *et al.*, a model RNA, U6–45, was designed for the present study (Fig. 2B). In addition to the RNA with the wild-type sequence, four mutants lacking some or all of the bulge-out residues were constructed, as shown in Fig. 3; each of the three bulged-out regions is deleted in M1-M3, and all of them were deleted in M4. We used fluorescein-labelled RNA for the competitive gel mobility shift assay. Combined with the use of the imaging analyzer, comparable sensitivity is obtained as with the method using radioisotopes.

The secondary structures of the model RNAs are analysed by enzymatic probing with RNase T_1, RNase T_2 and RNase V_1. The digestion patterns are shown in the Supplementary Fig. 1 and the results of digestion analysis are shown in Fig. 3. The UUCG loop region was digested by RNase T_1 and RNase T_2 equally for each RNA, indicating the formation of the loop structure. G7-A10 and A40-A41 in the stem region was digested by RNase V_1 equally for each RNA, indicating the formation of the stem structure. Thus, it was confirmed that each RNA forms the desired hairpin structure, although some differences were found around the bulged-out residues.

For U6–45, the stem between the bulged-out residues was digested weakly by RNase V_1, indicating that the region is flexible. M1 showed a similar digestion pattern with U6–45, except for the region around G12 and U14. This region was digested more than that of U6–45 by RNase V_1, indicating that the stem region became more stable, due to the removal of the bulged-out residue, A13. M2 also showed a similar pattern to that of the wild-type RNA, and again, the stem region was stabilized by the removal of A17. M3 lacking A31-G33 was cleaved by RNase T_2 at U14-A17, whereas RNase V_1 also cleaved the region, suggesting that M3 still forms a similar stem-bulge conformation with U6–45 and M1. In contrast, the analyses indicated that M4 forms a simple hairpin structure.

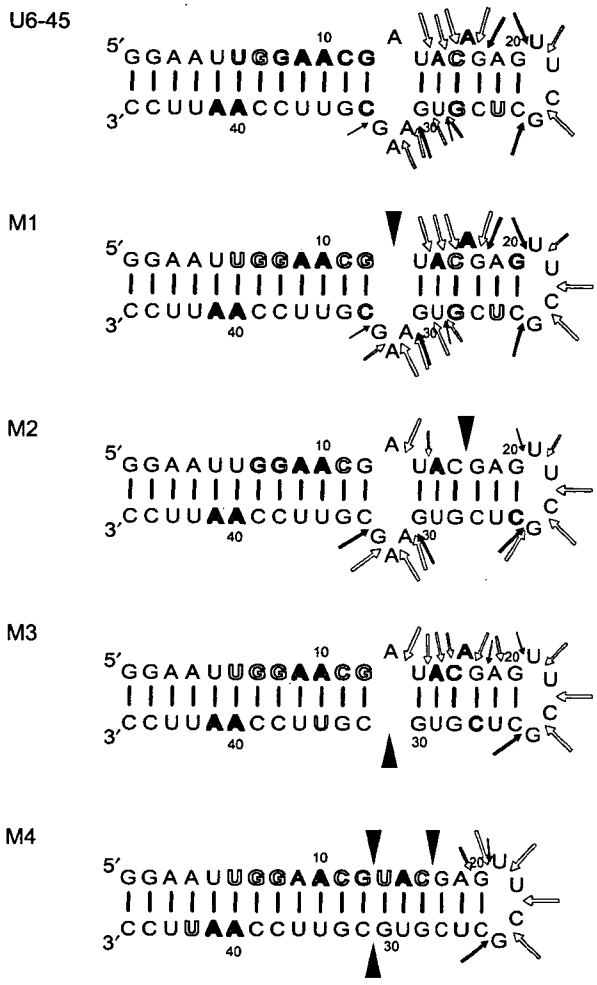

Fig. 3. **Results of RNase digestion analysis summarized on the secondary structures.** Filled and open arrows indicate the sites digested by RNase T_1 and T_2, respectively. Open characters indicate the sites digested by RNase V_1. For all cases, a larger arrow or character indicates stronger digestion. The mutation sites are indicated by arrows.

Binding of NS1 Protein to Model RNAs—To compare the binding affinities of the model RNAs to the NS1 protein, a competition assay was performed. The results of the self-competition assay using non-labelled U6–45 as competitor and fluorescein-labelled U6–45, are shown in Fig. 4. With the addition of the competitor RNA, the amount of labelled U6–45 in the complex was decreased, indicating that the competition works well. In contrast, with the addition of M1, lacking a bulged-out residue, the U6–45 complex could be observed even with a high concentration of the competitor RNA, indicating that M1 has lower affinity to the NS1 protein than U6–45 (Fig. 4B). This was also found for M3, as shown in Fig. 4D. M2, lacking the single bulged-out residue, also showed weak inhibition (Fig. 4C). However, M4 competed as well as U6–45 (Fig. 4E). Clearly, M4 recovers the NS1 binding affinity and M2 showed weaker binding, as compared to U6–45 and M4. From the analysis in Fig. 4, the dissociation constants for U6–45 and M4 to the NS1 protein were both estimated to be 2×10^{-9} M. The ratio of complex and free-labelled RNAs is summarized in the Supplementary Fig. 2.

Design of Peptide Derived from NS1 Protein and Gel Shift Assay—The RNA binding domain of NS1 protein consists of three α-helices as shown in Fig. 1A. Helix-1, -2 and -3 contain 2, 6 and 3 basic amino acid residues, respectively, and the basic amino acid residues except for Arg19, located in the helix-1, are exposed to solvent in the structures of NS1(1–73) (*18*, *19*). Thus, it is expected that the helix-2 is responsible for the RNA binding. This is consistent with the fact that Arg38 and Lys41 located in the helix-2 are involved in direct RNA binding (*26*). Accordingly, a peptide, NS1–2, derived from the helix-2 was constructed. The other peptide, NS1–3, derived from helix-3, was also constructed as a reference. In order to increase the water solubility, hydrophobic residues located inside of the NS1 protein were replaced by alanine residues in the designed peptides as show in Fig. 1B. Both of helix-2 and -3 are amphiphilic and the replaced leucine and isoleucine residues are located in the hydrophobic side of the helices (Supplementary Fig. 3). Both peptides showed enough water solubility to be used even for the NMR measurements. None of αH proton signals were observed in the lower magnetic field

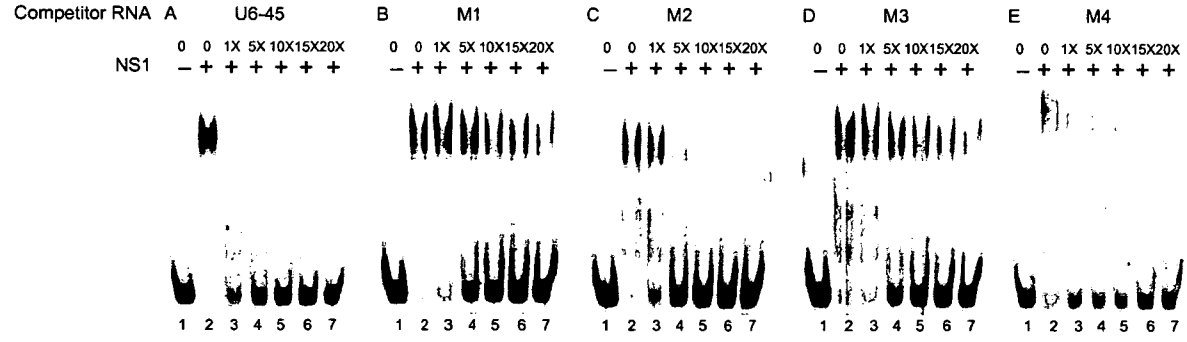

Fig. 4. **Competitive gel shift assay.** Each lane contains 0.05 μM of U6–45. Lanes 2–7 each contain 0.12 μM of NS1 protein. Lanes 3–7 contain 0.05, 0.25, 0.5, 0.75 and 1.0 μM of competitor RNA, respectively. The competitor RNAs are indicated for each panel.

than the signal of water (data not shown), suggesting that two peptides do not form a β strand. The free peptides might form a random coil structure because no NOEs indicating the formation of the α-helix were observed.

A shorter model RNA consisting of 34 nucleotide residues, U6–34, was designed for NMR measurements (Fig. 2C). The conformation of the model RNA was confirmed to be the predicted hairpin structure by PAGE and NMR analyses as described below. Binding of the peptides to the model RNA, U6–34, was analysed by the gel shift assay and the result was shown in Fig. 5. It is noted that no band corresponding to the dimer duplex was observed for the free RNA (Lane 1). By adding NS1–2, the band of U6–34 in the free state was decreased and the band of U6–34 in the complex was observed, indicating that NS1–2 binds to U6–34 (Lanes 2–4). The band of the complex was smear due to the dissociation of the peptide during the run, indicating the affinity is weak. In contrast, NS1–3 did not bind to U6–34 (Lanes 5–7). Thus, it is clearly confirmed that the helix-2 of NS1 protein is responsible for the RNA binding at least for the U6 snRNA. The free RNA band was still observed in the lane 2 in Fig. 5, containing 0.05 mM of RNA and 0.25 mM of peptide and the dissociation constant was estimated to be 10^{-4}–10^{-5} M.

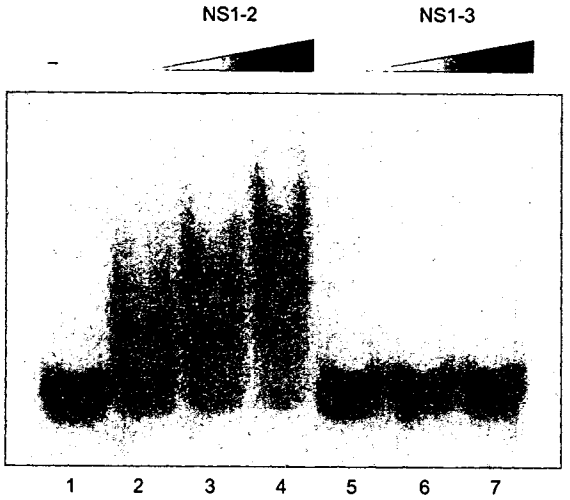

Fig. 5. **Gel shift assay for the RNA-binding ability of the peptides.** RNA samples were analysed by non-denaturing PAGE. The concentration of RNA was 0.05 mM for each lane in 5 μl of the loading buffer. Lane 1 is RNA alone. Lanes 2–4 (5–7) contain 0.25, 0.5 and 1.0 mM of NS1–2 (NS1–3).

NMR Analysis of U6–34—In order to elucidate the NS1–2 recognition site of U6–34, we conducted NMR experiments. Imino proton signals were assigned by using the 2D NOESY spectrum. NMR signals of H5/H6 of pyrimidine and H8 of purine, and ribose H1′ protons of U6–34 were assigned with the conventional method (*27*) by mainly using the 2D NOESY and 2D TOCSY spectra. Semi-selective [^{13}C/^{15}N] RNAs were used to confirm the assignment especially for residues in the bulge-out region.

The bottom spectrum of Fig. 6A corresponds to the free RNA and characteristic signals for the UUCG loop were observed at 11.5 and 10.4 ppm (*28*), indicating that U6–34 forms the desired hairpin structure. For each of G7 and G8, two imino proton signals were observed due to heterogeneity of the 3′ terminal which commonly happens in the transcription reaction with the T7 RNA polymerase. Sharp imino proton signals were not

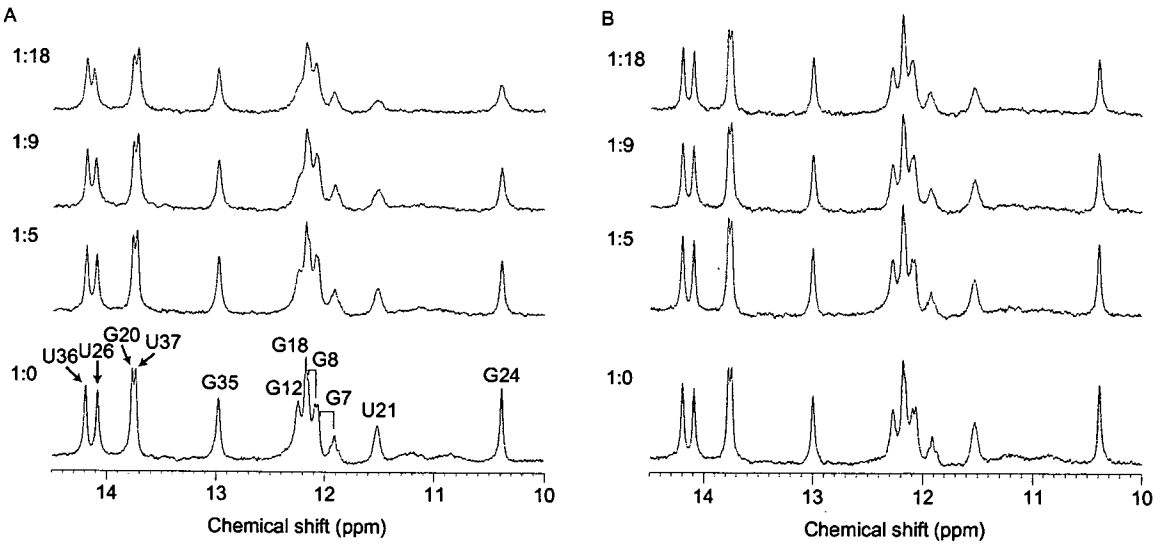

Fig. 6. **Peptide titration of imino proton spectra of U6–34.** The concentration of U6–34 was 0.1 mM and the molar ratios of U6–34 and NS1–2 (A) or NS1–3 (B) were indicated for each row. The signal assignments are shown in the bottom row of (A). A total of 600 MHz ^{1}H-NMR spectra were measured at a probe temperature of 22°C. For each experiment, 400 of scans were accumulated and 3.0 Hz of line broadening was applied prior to the Fourier transformation.

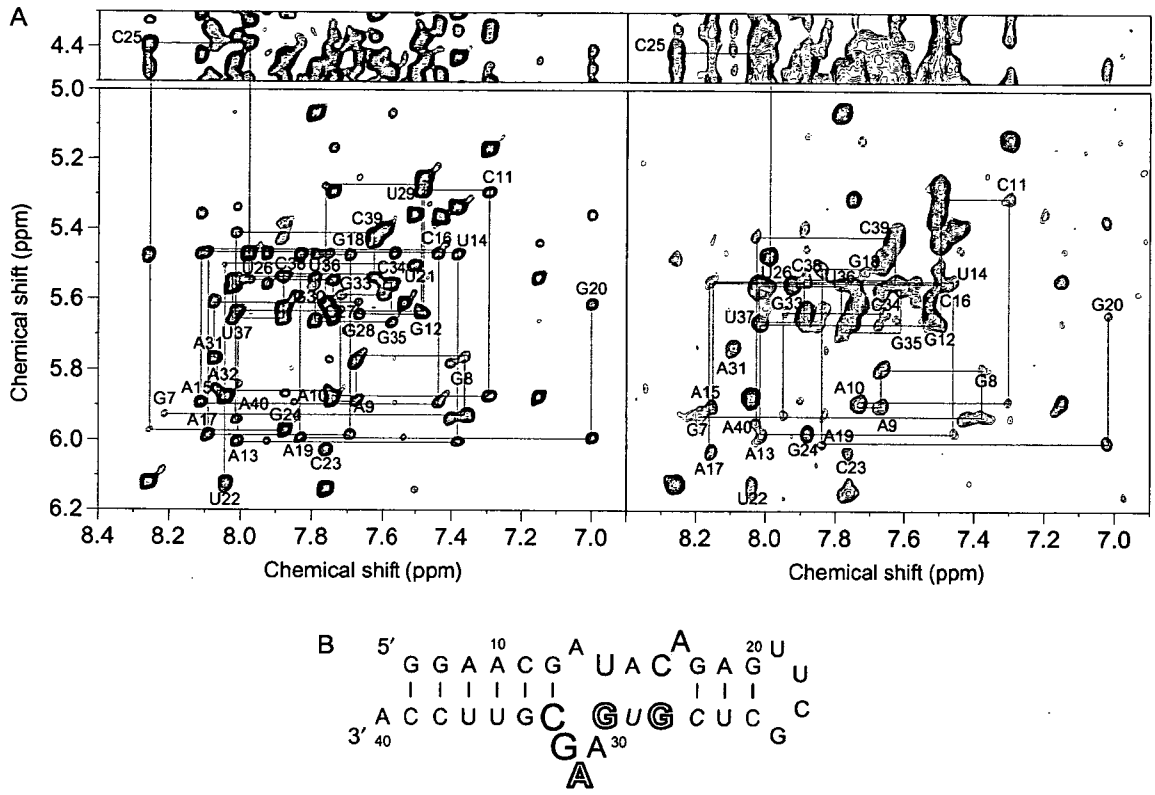

Fig. 7. **Chemical shift perturbation of U6–34 upon binding of NS1–2.** For the complex, the concentrations of U6–34 and NS1–2 were 0.1 and 1.8 mM, respectively. (A) 2D NOESY spectra of U6–34 in the absence (left) and presence (right) of NS1–2. The NOE connectivity is depicted by lines. The residue number labels indicate intra residue H6/H8-H1′ cross peaks. (B) Mapping of the chemical shift change on the secondary structure. Medium characters indicated the residues whose chemical shifts were changed by 0.05–0.1 ppm. Large characters indicated the residues with chemical shift changes of 0.1 ppm or more. Open large characters indicated the residues with large shifts or disappearances. Italic fonts indicate the residues that could not be assigned in the complex.

observed for the regions including residues U14-C16 and G28-G30 between the bulge-out residues. The NOE between H2 of A15 and H1′ of G30 which is the typical NOE for a regular A-type stem was not observed, whereas the NOEs between H2 of A31 and H1′ of C16 as well as H2 of A32 and H1′ of A15 were observed, suggesting the interaction between A31 and A15 as well as A32 and U14. Thus it was indicated that the regular A-type stem structure is not formed in this region as shown in Fig. 2C.

NMR Analysis of Interaction between NS1–2 and U6–34—By adding the NS1–2 to U6–34, most imino proton signals including G12, G18, G20, U21, G24 and U26 were broadened and some signals including U26 were slightly, by less than 0.1 ppm, shifted (Fig. 6A). In contrast, addition of NS1–3 did not change the imino proton signals (Fig. 6B). These results are consistent with that of the gel shift assay: NS1–2 binds to U6–34 but NS1–3 does not. Simultaneously, the results suggest that the NS1–2 binds to the bulge-out region but not to the stems or the UUCG loop. The concentration of the RNA and peptides were 0.1 and 1.8 mM, respectively, for the top spectrum of Fig. 6A, which were higher than those for lane 4 in Fig. 5, indicating that most of the RNA forms the complex.

We further analysed the effect of NS1–2 on the NMR signals of U6–34. Figure 7A shows the difference of the NOESY spectra of U6–34 in the absence (left) and presence (right) of NS1–2. For the spectra with NS1–2, the concentration of the RNA and peptides were 0.1 and 1.8 mM, respectively. Most of non-exchangeable proton signals were not changed upon addition of NS1–2 except for signals due to residues U14-A17 and G28-C34. Signals due to G33 shifted by more than 0.1 ppm and, furthermore, signals due to H8 and H1′ of G28 and G30 and H8 signal of A32 could not be assigned in the complex due to a large shift or disappearance. Residues G28-C34 showed a larger shift or broadening than residues U14-A17. These results were summarized in Fig. 7B and it was found that NS1–2 binds to the bulge-out region including the residues U14-A17 and G28-C34. It is noted that H1′ signals of C27 or U29 were not assigned in the complex due to an overlap with other signals.

DISCUSSION

RNA–protein interactions are important in many cellular processes. Recent structural studies of RNA–protein complexes have revealed that many specific contacts

are made between amino acids and nucleotides (*29*). In some cases, small peptides derived from RNA binding proteins such as Rev and Tat can recognize the specific sequence/structure of RNA molecules. Human immunodeficiency virus type-1 Rev peptide, consisting of 23 amino acids, forms an α-helix and recognizes an internal loop region of RRE RNA (*30*). Bovine immunodeficiency virus Tat peptide, consisting of 14 amino acids, forms a β-turn and recognizes dsRNA with bulge-out residues playing major roles (*31*). These small peptides provided excellent model systems for structural analysis of RNA–protein interaction by NMR spectroscopy. A detailed structural understanding of the interactions in the complex may assist in the design of therapeutics for viral disease.

Most RNA-binding proteins bind to their specific RNA by recognizing its characteristic structure; the HIV Tat protein specifically recognizes TAR RNA, and the HIV Rev protein recognizes the RRE (*30–32*). In contrast, the NS1 protein recognizes several kinds of RNAs, as described above. Thus, it is interesting to elucidate how such a small protein recognizes different kinds of RNAs. Since the NS1 protein weakly and non-specifically binds to RNAs, we used a competitive gel shift assay, rather than a simple gel shift assay, to analyse the specific RNA binding by the NS1 protein, which clearly revealed the different specificities of the NS1 protein for two kinds of RNAs, RNA containing a bulge and dsRNA. Before performing the competitive gel shift assay, we checked the conformations of the prepared RNA samples. The structural probing experiment showed that the stem-bulge region of the model RNAs designed in this study formed the expected secondary structures.

The competition assay showed that the deletion of each bulged-out region, A13 or A31-G33, decreased the binding affinity to the NS1 protein, suggesting that these residues are required for the NS1 protein binding. A17 is less important for the binding than A13 and A31–33, but is still required for efficient binding. Although it is not clear which residue directly interacts with the NS1 protein, we would expect that the specific structure of U6–45 is required for recognition by the NS1 protein. On the other hand, the simultaneous deletion of all of the bulged-out residues restored the binding affinity. Although the NS1 protein binding to dsRNA has already been documented (*12*, *13*), the fact that dsRNA competes with U6–45 for the NS1 protein binding is important. Together with the fact that the RNA binding domain of the NS1 protein is as small as about 70 residues, even though it forms a dimer, the NS1 binding sites for U6 snRNA and dsRNA seem to be identical or, at least, overlapped. This is consistent with the fact that the Arg38 and Lys41 residues, located in helix 2 of the NS1 protein, are involved in the interaction with U6 snRNA and dsRNA (*26*). It was also indicated that M1, M2 and M3, as well as U6–45, were not recognized as dsRNAs. Probably, the double-stranded part of U6–45 is too short to be recognized as dsRNA by the NS1 protein. In fact, Yin *et al.* recently showed the structural model of NS1-dsRNA complex in which 16bp RNA is recognized by the protein (*33*). The weak affinity of M1, M2 and M3 for the NS1 protein might be due to the similar conformation of U6–45, with its shorter double-stranded region, or to non-specific affinity.

The NS1 protein binds to poly(A) and influenza viral RNA, as described above. Hatada *et al.* suggested that the A bulge, in a double helix in viral RNA, is the NS1 binding site (*15*). A common feature of the three RNAs, poly(A), viral RNA and U6 snRNA, is the stretch of 'bulged-out' A residues with a specific spatial arrangement. Therefore, we can conclude that the NS1 protein recognizes either the stretch of 'bulged-out' A residues or dsRNA.

Two peptides consisting of 18 amino acid residues were designed and their RNA binding activities were analysed. Both helices-2 and -3 of NS1 proteins are amphiphilic and the leucine and isoleucine residues are located on the hydorophobic side of the helices and we replaced some of the hydrophobic residues to increase the water solubility (Supplementary Fig. 3). Because these hydrophobic residues are located inside of the protein in the structures of the RNA binding domain of NS1 protein (*18*, *19*), the replacements were expected to be silent for the RNA binding activity. As expected, NS1–2 containing six basic residues bound to U6–34, whereas NS1–3 containing three basic residues did not. Probably, three basic residues are too few to have an effective RNA binding activity. In fact, the Rev and Tat peptides contain 11 basic residues out of 23 residues and 7 out of 14, respectively (*30*, *31*).

A chemical shift perturbation technique is often used to observe the interaction between two biomolecules. The surface of the molecule that is interactive can be confirmed by the change of the NMR signal. However, the signals are changed even by the influence of the structural change caused by the formation of the complex. Thus, great care must be taken to interpret the interaction-induced chemical shift perturbation. It should be noted that Spitzfaden *et al.* (*34*) have shown that although perturbed resonances give good initial estimates of a binding surface, the effects extend beyond the direct contact area. The most likely explanation of the results of the chemical shift perturbation analysis in this study is that the NS1–2 binding site of U6–34 is mainly the RNA strand consisting of G28-C34 in the bulge-out region, including the bulged A31 and A32. The structure of the opposite strand consisting of U14-A17 might be changed upon the binding. Probably, NS1–2 binds to the major groove side of the bulge-out region as is the case with other arginine-rich peptides such as Rev and Tat. NS1–2 might form α-helix upon binding to U6–34 due to its amphiphilic nature. The observed broadenings of imino proton resonances corresponding to the base pairs adjacent to the bulge-out region, G12-C34 base pair, are probably due to the NS1–2 binding to the bulge-out region. The imino proton signals due to U21 and G24 of the UUCG loop also broadened upon binding of NS1–2. This is probably due to the partial disruption of the stem consisting of G18-G20 and C25-C27 upon binding of NS1–2 to the adjacent bulge-out region.

In conclusion, it was shown that the NS1 protein recognizes either the stretch of 'bulged-out' A residues or dsRNA. Further, NS1–2 peptide binds to G28-C34 in the bulge-out region of U6-34, including the bulged A31 and A32, suggesting that NS1 protein also bind to the 'bulged-out' A residues in a similar manner.

Supplementary data are available at *JB* online.

We thank Dr S. Nakada (Yamanouchi Pharmaceutical Co.) for advice and for providing the plasmid encoding NS1 protein, and Drs E. Hatada and R. Fukuda (Kanazawa University Graduate School of Medical Science) for giving us NS1 protein samples. We thank Dr K. Takai and Mr R. Ouchi for a kind gift of T7 RNA polymerase and Drs T. Sakamoto and N. Nameki for critical readings of the manuscript. This work was supported by 'Research for the Future' Program (JSPS-RFTF97L00503) from the Japan Society for the Promotion of Science and by a Grant-in-Aid for High Technology Research from Ministry of Education, Science, Sports and Culture, Japan.

REFERENCES

1. Buonagurio, D.A., Nakada, S., Parvin, J.D., Krystal, M., Palese, P., and Fitch, W.M. (1986) Evolution of human influenza A viruses over 50 years: rapid, uniform rate of change in NS gene. *Science* **232**, 980–982
2. Norton, G.P., Tanaka, T., Tobita, K., Nakada, S., Buonagurio, D.A., Greenspan, D., Krystal, M., and Palese, P. (1987) Infectious influenza A and B virus variants with long carboxyl terminal deletions in the NS1 polypeptides. *Virology* **156**, 204–213
3. Suarez, D.L. and Perdue, M.L. (1998) Multiple alignment comparison of the non-structural genes of influenza A viruses. *Virus Res.* **54**, 59–69
4. Nemeroff, M.E., Qian, X.-Y., and Krug, R.M. (1995) The influenza virus NS1 protein forms multimers in vitro and in vivo. *Virology* **212**, 422–428
5. Qian, X.-Y., Chien, C.-Y., Lu, Y., Montelione, G.T., and Krug, R.M. (1995) An amino-terminal polypeptide fragment of the influenza virus NS1 protein possesses specific RNA-binding activity and largely helical backbone structure. *RNA* **1**, 948–956
6. Qian, X.-Y., Alonso-Caplen, F., and Krug, R.M. (1994) Two functional domains of the influenza virus NS1 protein are required for regulation of nuclear export of mRNA. *J. Virol.* **68**, 2433–2441
7. Aragón, T., de la Luna, S., Novoa, I., Carrasco, L., Ortín, J., and Nieto, A. (2000) Eukaryotic translation initiation factor 4GI is a cellular target for NS1 protein, a translational activator of influenza virus. *Mol. Cell. Biol.* **20**, 6259–6268
8. Qiu, Y. and Krug, R.M. (1994) The influenza virus NS1 protein is a poly(A)-binding protein that inhibits nuclear export of mRNAs containing poly(A). *J. Virol.* **68**, 2425–2432
9. Lu, Y., Qian, X.-Y., and Krug, R.M. (1994) The influenza virus NS1 protein: a novel inhibitor of pre-mRNA splicing. *Genes & Dev* **8**, 1817–1828
10. Qin, Y., Nemeroff, M., and Krug, R.M. (1995) The influenza NS1 protein binds to a specific region in human U6 snRNA and inhibits U6-U2 and U6-U4 snRNA interactions during splicing. *RNA* **1**, 304–316
11. Wang, W. and Krug, R.M. (1998) U6atac snRNA, the highly divergent counterpart of U6 snRNA, is the specific target that mediates inhibition of AT-AC splicing by the influenza virus NS1 protein. *RNA* **4**, 55–64
12. Hatada, E. and Futada, R. (1992) Binding of influenza A virus NS1 protein to dsRNA in vitro. *J. Gen. Virol.* **73**, 3325–3329
13. Lu, Y., Wambach, M., Katze, M.G., and Krug, R.M. (1995) Binding of the influenza virus NS1 protein to double-stranded RNA inhibits the activation of the protein kinase that phosphorylates the eIF-2 translation initiation factor. *Virology* **214**, 222–228
14. Min, J.Y. and Krug, R.M. (2006) The primary function of RNA binding by the influenza A virus NS1 protein in infected cells: Inhibiting the 2′-5′ oligo (A) synthetase/RNase L pathway. *Proc. Natl. Acad. Sci. USA* **103**, 7100–7105
15. Hatada, E., Saito, S., Okishio, N., and Fukuda, R. (1997) Binding of the influenza virus NS1 protein to model genome RNAs. *J. Gen. Virol* **78**, 1059–1063
16. Marlón, R.M., Aragón, T., Belose, A., Nieto, A., and Ortín, J. (1997) The N-terminal half of the influenza virus NS1 protein is sufficient for nuclear retention of mRNA and enhancement of viral mRNA translation. *Nucleic Acids Res.* **25**, 4271–4277
17. Park, Y.W. and Katze, M.G. (1995) Translational control by influenza virus. Identification of cis-acting sequences and trans-acting factors which may regulate selective viral mRNA translation. *J. Biol. Chem* **270**, 28433–28439
18. Chien, C.-Y., Tejero, R., Huang, Y., Zimmerman, D.E., Ríos, C.B., Krug, R.M., and Montelione, G.T. (1997) A novel RNA-binding motif in influenza A virus non-structural protein 1. *Nature Struc. Biol.* **4**, 891–895
19. Liu, J., Lynch, P.A., Chien, C.-Y., Montelione, G.T., Krug, R.M., and Berman, H.M. (1997) Crystal structure of the unique RNA-binding domain of the influenza virus NS1 protein. *Nature Struc. Biol.* **4**, 896–899
20. Kramer, A. (1996) The structure and function of proteins involved in mammalian pre-mRNA splicing. *Annu. Rev. Biochem.* **65**, 367–409
21. Harada, F., Kato, N., and Nishimura, S. (1980) The nucleotide sequence of nuclear 4.8S RNA of mouse cells. *Biochem. Biophys. Res. Commun.* **95**, 1332–1340
22. Rinke, J., Appel, B., Digweed, M., and Lührmann, R. (1985) Localization of a base-paired interaction between small nuclear RNAs U4 and U6 in intact U4/U6 ribonucleoprotein particles by psoralen cross-linking. *J. Mol. Biol.* **185**, 721–731
23. Young, J.F., Desselberger, U., Palese, P., Ferguson, B., Shatzman, A.R., and Rosenberg, M. (1983) Efficient expression of influenza virus NS1 nonstructural proteins in *Escherichia coli*. *Proc. Natl. Acad. Sci. USA* **80**, 6105–6109
24. Pardi, A. and Nikonowicz, E.P. (1992) Simple procedure for resonance assignment of the sugar protons in ^{13}C labeled RNA. *J. Am. Chem. Soc.* **114**, 9202–9203
25. Legault, P., Farmer, B.T., II., Mueller, L., and Pardi, A. (1994) Through-bond correlation of adenine protons in a ^{13}C-labeled ribozyme. *J. Am. Chem. Soc.* **116**, 2203–2204
26. Wang, W., Riedel, K., Lynch, P., Chien, C.-Y., Montelone, G.T., and Krug, R.M. (1999) RNA binding by the novel helical domain of the influenza virus NS1 protein requires its dimer structure and a small number of specific basic amino acids. *RNA* **5**, 195–205
27. Wüthrich, K. (1986) *NMR of Proteins and Nucleic Acids* John Wiley & Sons. Inc., New York
28. Varani, G., Chenog, C., and Tinoco, I., Jr. (1991) Structure of an unusually stable RNA hairpin. *Biochem.* **30**, 3280–3289
29. Frankel, A.D. (2000) Fitting peptides into the RNA world. *Curr. Opin. Stuct. Biol.* **10**, 332–340
30. Battiste, J.L., Mao, H., Rao, N.S., Tan, R., Muhandiram, D.R., Kay, L.E., Frankel, A.D., and Williamson, J.R. (1996) Alpha helix-RNA major groove recognition in an HIV-1 rev peptide-RRE RNA complex. *Science* **273**, 1547–1551
31. Puglisi, J.D., Chen, L., Blanchard, S., and Frankel, A.D. (1995) Solution structure of a bovine immunodeficiency virus Tat-TAR peptide-RNA complex. *Science* **270**, 1200–1203
32. Ye, X., Kumar, R.A., and Patel, D.J. (1995) Molecular recognition in the bovine immunodeficiency virus Tat peptide-TAR RNA complex. *Chem. Biol.* **12**, 827–840

33. Yin, C., Khan, J.A., Swapna, G.V.T., Ertekin, A., Krug, R.M., Tong, L., and Montelione, G.T. (2007) Conserved surface features form the double-stranded RNA binding site of non-structural protein 1 (NS1) from influenza A and B viruses. *J. Biol. Chem.* **82**, 20584–20592

34. Spitzfaden, C., Weber, H.P., Braun, W., Kallen, J., Wider, G., Widmer, H., Walkinshaw, M.D., and Wüthrich, K. (1992) Cyclosporin A-cyclophilin complex formation. A model based on X-ray and NMR data. *FEBS Lett.* **300**, 291–300

The Tax protein of HTLV-1 promotes oncogenesis in not only immature T cells but also mature T cells

To the editor:

Adult T-cell leukemia/lymphoma (ATLL) is a fatal T-cell neoplasm caused by infection with human T-cell leukemia virus type I (HTLV-I). Hasegawa *et al.*[1] have described transgenic mice that express HTLV-I Tax viral regulatory protein/oncoprotein in thymocytes. These mice developed pre–T-cell ($CD4^-CD8^-$) lymphoma and leukemia. This is the first report that Tax alone is sufficient to promote oncogenesis in T cells. Tax is encoded by the *pX* region in HTLV-I, and is thought to play a central role in the leukemogenesis of ATLL (ref. 2). Transgenic mice expressing Tax develop tumors, but until the report of Hasegawa *et al.*[1], none of these mice had been reported to develop ATLL-like T-cell lymphoma or leukemia[3]. The lymphoma cells in the transgenic mice developed by Hasegawa *et al.*[1], however, were immature T cells, whereas oncogenic cells in ATLL are generally mature lymphocytes[4].

We have developed a transgenic mouse model of HTLV-I by using a mouse lymphocyte–specific protein-tyrosine kinase (Lck) distal promoter[5] to express the *Tax* gene in mature thymocytes and peripheral T lymphocytes. These mice were maintained under pathogen-free conditions, and, by the age of 21 months, 22% (14 of 63) had developed T-cell leukemia/lymphoma. The mice developed marked splenomegaly, hepatomegaly and lymphadenopathy (**Fig. 1a**). Total white blood cell count in transgenic mice with lymphoma was markedly elevated compared with that in nontransgenic mice. Large and abnormal leukemic cells comprised >80% of the peripheral blood mononuclear cells in a blood smear (**Fig. 1b**, left panel). We also observed a 'flower cell' morphology, albeit at low incidence (<5%) (**Fig. 1b**, right panel). Histological examination showed diffuse, large-cell lymphomas in the spleen, lymph nodes, liver, thymus, bone marrow, kidney, lung, meninges and skin (**Fig. 1c,d**).

On the basis of our pathological and histopathological findings, the disease presented by our transgenic mice corresponds to pre–T-cell leukemia/lymphoma, as defined in the transgenic mice reported by Hasegawa

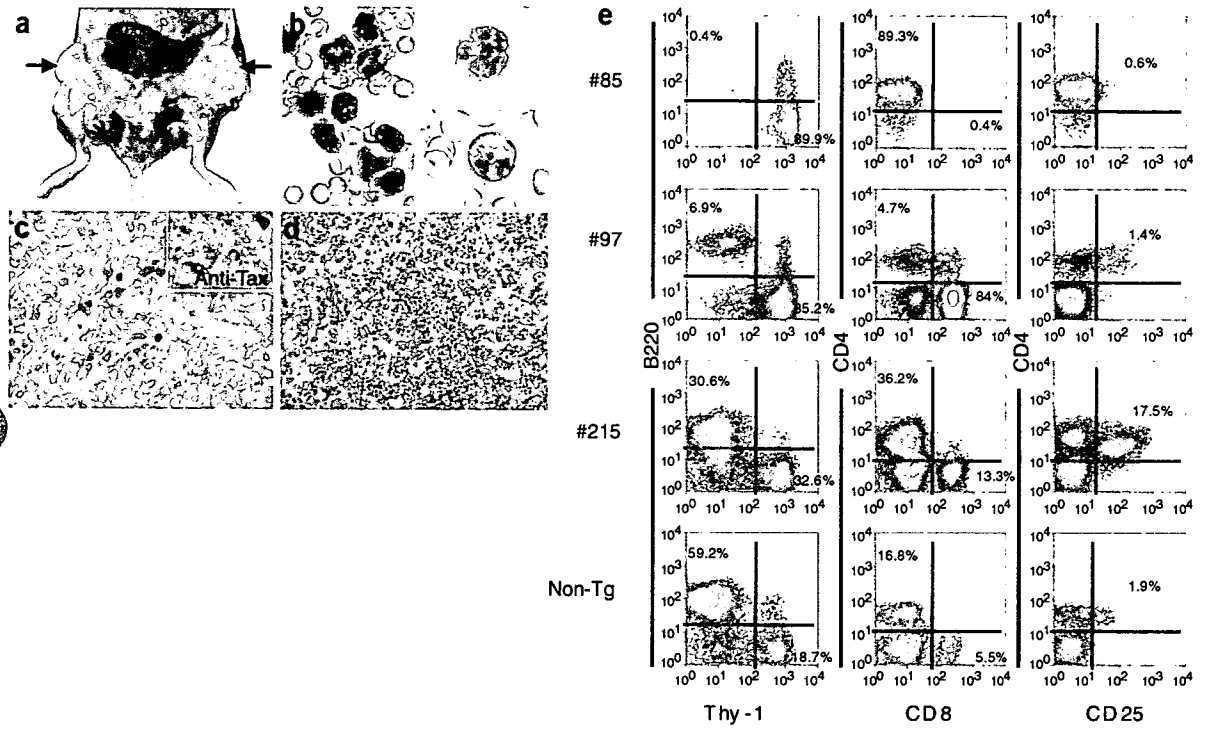

Figure 1 Pathological findings and flow cytometric analysis of lymphoma cells in Tax transgenic mice. (**a**) Marked splenomegaly, hepatomegaly and lymphadenopathy. (**b**) Left, peripheral blood smears from transgenic (Tg) mouse #85 with a high white blood cell count (178,000 mm^3). Right, leukemic cells with multilobulated nuclei, the 'flower cell' morphology. (**c**) H&E staining shows diffuse large-cell lymphoma in an inguinal lymph node. Inset, immunohistochemical staining with antibodies to Tax. The anti-Tax/HTLV-I Tax hybridoma 168A51-42 (Tab176) was obtained from B.C. Langton (through the AIDS Research and Reference Reagent Program, Division of AIDS, National Institute of Allergy and Infectious Diseases, US National Institutes of Health). (**d**) Histology (H&E staining) shows infiltration of leukemic cells in the liver. (**e**) Flow cytometry reveals the phenotype of leukemic cells using the indicated fluorescence marker–conjugated antibodies. All data were gated for viable cells. Percentages represent proportions of viable cells in each region or quadrant. Phenotype of lymph node cells from mice #85 and #97 were $CD4^+$ and $CD8^+$, respectively. Both leukemic cells from #85 and #97 were negative for CD25. In mouse #215, expression of Thy-1 in cells, which confirmed their identity as $CD4^+CD25^+$ T cells, was elevated compared with that in control mice (17.5% versus 1.9%). Spleen cell suspensions from a littermate (non-Tg) of mouse #85 were used as a control. Both #85 and the littermate control mouse were 9 months old. Mice #97 and #215 were 8 and 20 months old, respectively. All procedures involving animals and their care were approved by the animal care committee of Kumamoto University in accordance with Institution and Japanese government guidelines (Guidelines for Proper Conduct of Animal Experiments, Science Council of Japan, and the Law for the Humane Treatment and Management of Animals).

et al.[1]. Thus, we further characterized the leukemic cells in our transgenic mice. Flow cytometry revealed that the major phenotype of the leukemic cells was $CD4^+$ or $CD8^+$ T cells and that these T cells were mature (**Fig. 1e**). Thus, one major difference between our model and that reported by Hasegawa *et al.*[1] is the maturation stage of T cells in the leukemic cells. Our results provide additional support for the hypothesis that HTLV-I Tax promotes oncogenesis not only in immature T cells, as reported by Hasegawa and his colleagues[1], but also in mature T cells.

Tax has been shown *in vitro* to induce the expression of a variety of host genes, including those encoding interleukin (IL)-2 and the α-chain of the IL-2 receptor (IL-2R/CD25)[6,7]. Although it is generally agreed that activation of the IL-2/IL-2R (CD25) loop contributes to T-cell activation and proliferation—with subsequent events leading to malignant transformation in ATLL—there is little *in vivo* evidence for the expression of IL-2 by HTLV-I–infected T cells. In our mouse model, the clonal phenotype of malignant cells was either $CD4^+$ or $CD8^+$, but $CD25^-$, whereas ATLL usually exhibits a $CD4^+CD25^+$ T-cell phenotype[4]. It is unclear why the transgenic leukemia cells did not express CD25, although the expression of Tax in these cells was very high (**Fig. 1c**, inset). To date, we have observed $CD4^+CD25^+$ T-cell proliferation during polyclonal expansion of leukemia cells in only one of 63 mice tested up to the age of 21 months (**Fig. 1e**, #215). It has been reported that the expression of IL-2R (CD25) in HTLV-I–infected T cells seems to be stimulated by IL-2, which is induced by parasite antigen in human carriers dually infected with *Strongyloides stercoralis* and HTLV-I (ref. 8). This report and our results for transgenic mice reared under pathogen-free conditions suggest that the expression of CD25 in proliferating $CD4^+CD25^+$ HTLV-I–infected T cells might require cofactors, such as other infectious agents, that produce IL-2.

Takeo Ohsugi[1], Toshio Kumasaka[2], Seiji Okada[3] & Toru Urano[1]

[1]Division of Microbiology and Genetics, Center for Animal Resources and Development, Institute of Resource Development and Analysis, Kumamoto University, 2-2-1 Honjo, Kumamoto 860-0811, Japan. [2]Department of Pathology (I), Juntendo University School of Medicine, 2-1-1 Hongo, Bunkyo-ku, Tokyo 113-8421, Japan. [3]Center for AIDS Research, Kumamoto University, 2-2-1 Honjo, Kumamoto 860-0811, Japan.
e-mail: ohsugi@gpo.kumamoto-u.ac.jp

COMPETING INTERESTS STATEMENT
The authors declare no competing financial interests.

1. Hasegawa, H. *et al. Nat. Med.* **12**, 466–472 (2006).
2. Jeang, K.T., Giam, C.Z., Majone, F. & Aboud, M. *J. Biol. Chem.* **279**, 31991–31994 (2004).
3. Lairmore, M.D., Silverman, L. & Ratner, L. *Oncogene* **24**, 6005–6015 (2005).
4. Uchiyama, T. *Annu. Rev. Immunol.* **15**, 15–37 (1997).
5. Wildin, R.S., Wang, H.U., Forbush, K.A. & Perlmutter, R.M. *J. Immunol.* **155**, 1286–1295 (1995).
6. Siekevitz, M., Feinberg, M.B., Holbrook, N., Wong-Staal, F. & Greene, W.C. *Proc. Natl. Acad. Sci. USA* **84**, 5389–5393 (1987).
7. Cross, S.L. *et al. Cell* **49**, 47–56 (1987).
8. Satoh, M. *et al. Oncogene* **21**, 2466–2475 (2002).

Journal of Cellular Physiology

M-CSF-Mediated Macrophage Differentiation but not Proliferation Is Correlated with Increased and Prolonged ERK Activation

SHINYA SUZU,[1] MASATERU HIYOSHI,[1] YUKA YOSHIDOMI,[1] HIDEKI HARADA,[1] MOTOHIRO TAKEYA,[2] FUMIHIKO KIMURA,[3] KAZUO MOTOYOSHI,[3] AND SEIJI OKADA[1]*

[1]*Division of Hematopoiesis, Center for AIDS Research, Kumamoto University, Kumamoto, Japan*

[2]*Department of Cell Pathology, Graduate School of Medical and Pharmaceutical Sciences, Kumamoto University, Kumamoto, Japan*

[3]*Third Department of Internal Medicine, National Defense Medical College, Saitama, Japan*

M-CSF is a cytokine essential for both the proliferation and differentiation of monocytes/macrophages. In this study, we established a new M-CSF-mediated differentiation-inducing system, and examined how the level and duration of the activation of ERK preceded M-CSF-mediated differentiation. TF-1-fms human leukemia cells rapidly proliferated in response to M-CSF. However, in the presence of a phorbol ester, TPA, TF-1-fms cells definitely switched their responsiveness to M-CSF from proliferation to differentiation, as evidenced by a more drastic morphological change and the appearance of cells with a higher level of phagocytic activity. In TF-1-fms cells expressing HIV-1 Nef protein in a conditionally active-manner, both M-CSF-mediated proliferation and M-CSF/TPA-mediated differentiation were inhibited by the activation of Nef. The Nef-active cells showed perturbed patterns of ERK activation. Under the proliferation-inducing conditions (TPA-free), parental or Nef-inactive cells showed modest ERK activation following M-CSF stimulation, whereas Nef-active cells showed an earlier and transient ERK activation, despite a decrease in their proliferation rate. Under the differentiation-inducing conditions, parental or Nef-inactive cells showed increased and prolonged ERK activation following M-CSF stimulation, whereas Nef-active cells showed transient ERK activation. These results supported the idea that the increased and prolonged ERK activation led to M-CSF-mediated macrophage differentiation but not to proliferation.

J. Cell. Physiol. 212: 519–525, 2007.

Macrophage colony-stimulating factor (M-CSF) is a cytokine that supports both proliferation and differentiation of the cells of monocytic lineage (Roth and Stanley, 1992). The biological effects of M-CSF are mediated by a receptor tyrosine kinase, Fms (Sherr et al., 1985). The binding of M-CSF leads to the autophosphorylation of tyrosine residues in the cytoplasmic domain of Fms and subsequent interactions of the phosphorylated residues with other proteins, resulting in the initiation of multiple pathways (Bourette and Rohrschneider, 2000). Thus, to investigate which pathway leads to the proliferation or differentiation, mutant Fms proteins in which the tyrosine residues are substituted with phenylalanine have been generated and expressed in various cell types, such as NIH3T3 fibroblasts (Roussel et al., 1990), Rat-2 fibroblasts (van der Geer and Hunter, 1993), FDC-P1 myeloid progenitor cells (Bourette et al., 1995) and M1 myeloid cells (Marks et al., 1999). However, because the pathway that is predominantly utilized and whether cells proliferate or differentiate in response to M-CSF depend on the cell type, the exact differences in the signaling events between these distinct cellular responses to M-CSF are still unclear. Culture systems in which the same cells distinctly respond to different stimuli (proliferation versus differentiation) are useful for clarifying this issue. For example, rat neuronal PC12 cells proliferate in response to EGF, whereas stimulation with NGF causes neuronal differentiation (Marshall, 1995). Of importance, studies with this culture system have revealed that the increased and prolonged activation of extracellular signal-regulated kinase (ERK) is critical for the neuronal differentiation of PC12 cells, but not for proliferation (Marshall, 1995). It has been also shown that the increased and prolonged activation of ERK is critical for the differentiation of megakaryocytes (Melemed et al., 1997; Racke et al., 1997) and muscle cells (Gredinger et al., 1998). Furthermore, the functional maturation of macrophages induced by lipopolysaccharide seemed to require increased and prolonged ERK activation (Valledor et al., 2000). However, the role of ERK activation in M-CSF-mediated macrophage differentiation is not fully understood.

In this study, we first attempted to establish a new M-CSF-mediated differentiation-inducing system, using human leukemia TF-1-fms cells which essentially showed a proliferative response to M-CSF (Suzu et al., 1997). We assessed whether 12-*O*-tetradecanoylphorbol 13-acetate (TPA) triggered their differentiation and M-CSF accelerated the process. TPA has been characterized by its ability to induce the differentiation of several leukemia cell lines (Kitamura et al., 1989; Racke et al., 1997; He et al., 1999). We next attempted to clarify whether

Contract grant sponsor: Ministry of Health, Labour and Welfare of Japan;
Contract grant number: H16-AIDS-003.

*Correspondence to: Seiji Okada, Division of Hematopoiesis, Center for AIDS Research, Kumamoto University, Honjo 2-2-1, Kumamoto-city, Kumamoto 860-0811, Japan.
E-mail: okadas@gpo.kumamoto-u.ac.jp

Received 15 June 2006; Accepted 10 January 2007

DOI: 10.1002/jcp.21045

the increased and prolonged activation of ERK preceded M-CSF-mediated differentiation, by utilizing TF-1-fms cells expressing a conditionally active HIV-1 Nef protein (Suzu et al., 2005). Previously, we showed that Nef activation inhibited the M-CSF-mediated proliferation of TF-1-fms cells but enhanced the activation of ERK following M-CSF treatment (Suzu et al., 2005). Nef is a major determinant of the pathogenicity of HIV-1 (Fackler and Baur, 2002; Peterlin and Trono, 2003; Qiao et al., 2006), and has been shown to bind to and activate Hck, a Src kinase (Saksela et al., 1995; Moarefi et al., 1997). The activation of Hck was one possible molecular mechanism by which Nef caused the inhibition of M-CSF-mediated cell proliferation (Suzu et al., 2005) and the enhancement of ERK activation (Schrager et al., 2002; He et al., 2004). Based on these findings, we carefully examined how Nef affected the M-CSF/TPA-mediated differentiation of TF-1-fms cells and the level/duration of ERK activation in the differentiation-inducing conditions.

Materials and Methods

Cell culture and reagents

TF-1 cells (Kitamura et al., 1989) were routinely cultured with RPMI 1640 medium (Sigma, St. Louis, MO) — 10% fetal calf serum (FCS) in the presence of recombinant human granulocyte/macrophage-CSF (GM-CSF) (2 ng/ml; PeproTech, London, UK). TF-1-fms cells (Suzu et al., 1997) were maintained with RPMI 1640 — 10% FCS in the presence of M-CSF (100 ng/ml; a gift from Morinaga Milk Industry, Kanagawa, Japan) and G418 (200 μg/ml; Life Technologies, Grand Island, NY). TF-1-fms cells expressing the HIV-1 Nef-murine estrogen receptor hormone-binding domain (Nef-ER) fusion protein (TF-1-fms-Nef-ER) (Walk et al., 2001; Suzu et al., 2005) were maintained with RPMI 1640 — 10% FCS containing M-CSF, G418, and puromycin (1.5 μg/ml; Sigma). In this system, Nef was basally inactive but its function was inducibly activated by the estrogen analogue, 4-hydroxytamoxifen (4-HT; Sigma) (Suzu et al., 2005). In this study, we also established TF-1 cells expressing the Nef-ER fusion protein with the plasmid pEBB-Nef-ER-IRES-puro (Walk et al., 2005). TF-1-Nef-ER cells were maintained with RPMI 1640 — 10% FCS containing GM-CSF and puromycin. To activate Nef, 4-HT was added to the culture at a final concentration of 1 μM. TPA (Sigma) was added to the culture at a final concentration of 100 ng/ml. PD98059 (ERK kinase inhibitor) and PP2 (Src kinase inhibitor) were purchased from Sigma. U0126 was purchased from Calbiochem (San Diego, CA).

Cell count and viability analysis

The viable cell counts were obtained by enumerating the cells that excluded trypan blue dye on a hemocytometer. The adherent cells were harvested by trypsinization. The viability of cells was also examined with the propidium iodide (PI) exclusion method (Okada et al., 1998). Cells were suspended in phosphate-buffered saline (PBS) containing 0.1% NaN_3, 3% FCS and 2 μg/ml PI. The uptake of PI in each cell was analyzed with a FACSCalibur using Cell Quest Software (Becton Dickinson, Mountain View, CA).

Analyses of expression of Fms and CD204, and phagocytic activity

The cell surface expression of Fms was analyzed by flow cytometry using Flag-tagged M-CSF (Suzu et al., 2005). In brief, cells were incubated with the Flag-tagged M-CSF followed by biotin-labeled anti-Flag M2 antibody (Sigma) and phycoerythrin (PE)-labeled streptavidin (PharMingen, San Jose, CA). The analyses were performed with a FACSCalibur. The cell surface expression of CD204 was determined using anti-CD204-FITC (clone E-5) (Tomokiyo et al., 2002). The phagocytic activity was determined by measuring the uptake of fluorescent microspheres (Fluoresbrite Carboxylate Microspheres, 0.7 μm in diameter, Polysciences, Warrington, PA). Cells cultured on a 6-well tissue culture plate were incubated with the fluorescent microspheres for 5 h and washed with PBS. The cells showing phagocytized particles were analyzed by flow cytometry.

Immunoprecipitation and Western blotting

The immunoprecipitation and Western blotting were performed essentially as described previously (Suzu et al., 2000, 2005). Cells were depleted of M-CSF for 14 h in RPMI 1640 — 10% FCS with or without TPA, and then stimulated with M-CSF for the indicated periods. In selected experiments, 4-HT was added to the culture at the initiation of M-CSF deprivation/TPA pre-treatment. Then, the cells were solubilized with the Nonidet P-40 lysis buffer. The immunoprecipitation was performed with anti-phosphotyrosine mouse IgG conjugated to agarose (PY99; Santa Cruz Biotechnology, Santa Cruz, CA). The antibodies (purchased from Santa Cruz) used for Western blotting were as follows: anti-Fms (C-20), anti-phosphotyrosine (PY99), anti-ERK (K-23), and anti-phosphorylated ERK (E-4). The rabbit antiserum to Nef was obtained from the NIH AIDS Research and Reference Reagent Program (Division of AIDS, NIAID, NIH, Bethesda, MD). The detection was performed using the ECL system (Amersham, Buckinghamshire, UK). The relative intensity of bands on scanned gel images was quantified by using the NIH Image software.

Results

Proliferative- and differentiative properties of TF-1-fms cells

TF-1-fms cells were derived from TF-1 cells by introducing the wild-type *c-fms* gene into the parental cells (Fig. 1A). The proliferation of TF-1 and TF-1-fms was entirely dependent on GM-CSF and M-CSF, respectively (Fig. 1B) (Kitamura et al., 1989; Suzu et al., 1997). TF-1-fms cells lost their responsiveness to GM-CSF, due to a loss of the expression of the GM-CSF receptor α chain (data not shown). In the presence of M-CSF, TF-1-fms cells neither adhered to dishes (Fig. 1C) nor showed a differentiated morphology (Fig. 1D, top part). On the other hand, when cultured with media containing TPA alone, the cells tended to adhere to dishes and show a flattened morphology (Figs. 1C and D, middle part). Of note, M-CSF accelerated the differentiation-like process. Most TF-1-fms cells cultured in the presence of both M-CSF and TPA adhered to dishes and showed a mature macrophage-like morphology (Figs. 1C and D, bottom part), which closely resembled the primary macrophages obtained by culturing human peripheral blood monocytes with M-CSF (Hashimoto et al., 1999). In parallel with the morphological change, these cells showed more of an increase in granularity than cells cultured with TPA alone (Fig. 1E). More importantly, these cells showed higher phagocytic activity: the percentage of cells phagocytizing the microbeads and their mean fluorescence intensity (MFI) were higher in the culture containing M-CSF and TPA than in the culture containing TPA alone (Fig. 1F, left part). In addition, these cells showed a higher level of CD204 (class A macrophage scavenger receptor) (Fig. 1F, right part). These results indicated that the cells obtained by culturing TF-1-fms cells with both M-CSF and TPA were functionally mature macrophages.
As mentioned above and shown in the upper panel of Figure 2A, the culture of TF-1-fms cells with TPA resulted in the appearance of adherent cells and the addition of M-CSF further increased the number of adherent cells. However, there was no significant difference in total number of viable cells between the two treatments (TPA alone versus M-CSF + TPA) (Fig. 2A, lower part). Moreover, there was no significant difference in the percentage of PI-positive dead cells between the two treatments (Fig. 2B), excluding the possibility that the acceleration of TF-1-fms cell differentiation by M-CSF and TPA reflected a survival-enhancing or anti-apoptotic function of M-CSF. It was therefore likely that TF-1-fms cells definitely switched their responsiveness to M-CSF from proliferation to macrophage differentiation in the presence of TPA.

Requirement of ERK activation for M-CSF-mediated proliferation and M-CSF/TPA-mediated differentiation of TF-1-fms cells

We next examined whether the activation of ERK was required for M-CSF-mediated proliferation and M-CSF/TPA-mediated

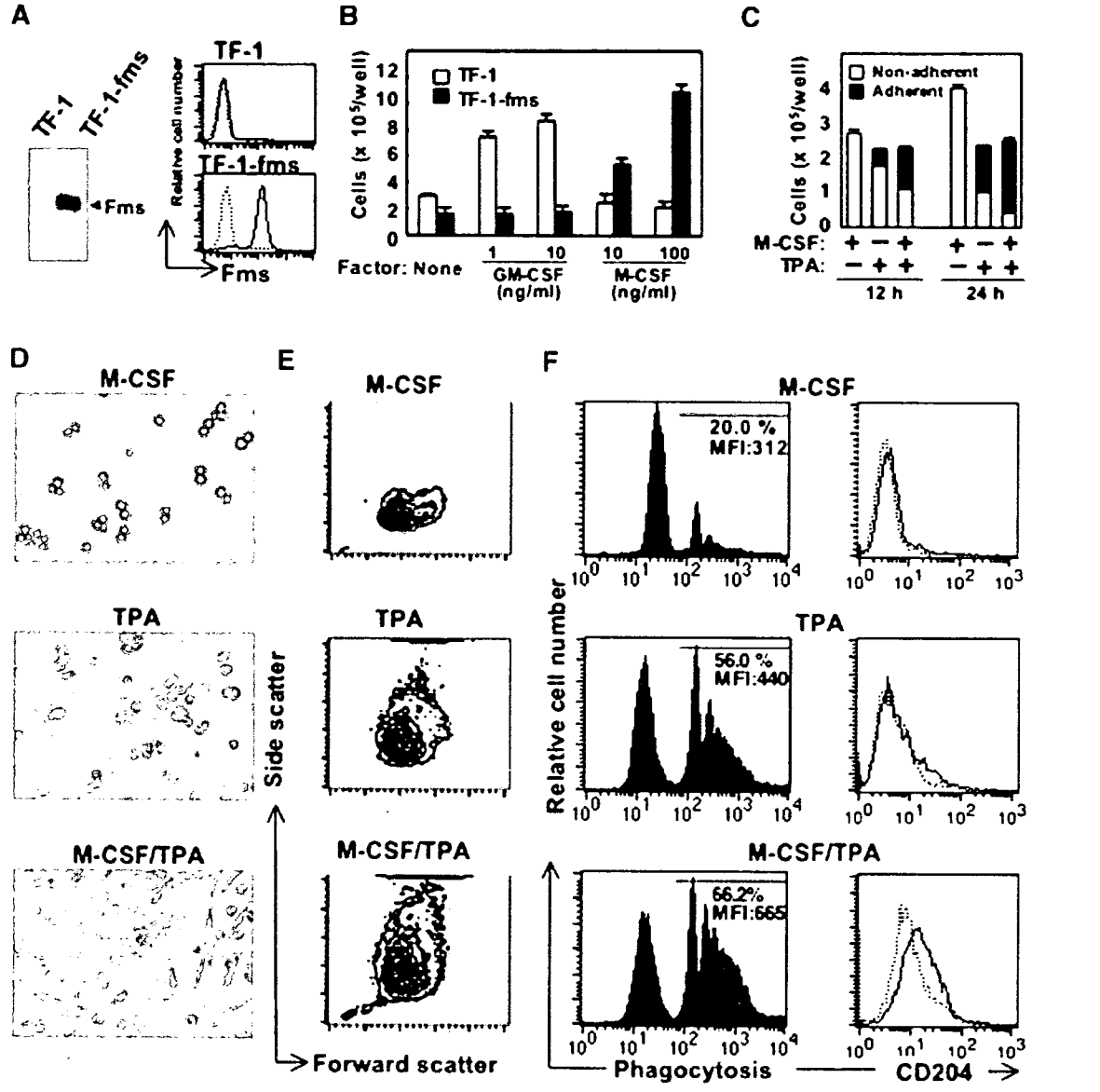

Fig. 1. The expression of Fms in and proliferative and differentiative properties of TF-1-fms cells. A: The total cell lysates from TF-1 or TF-1-fms cells were analyzed for the expression of Fms by Western blotting. Alternatively, the level of cell surface Fms expression was analyzed by flow cytometry with Flag-tagged M-CSF (solid lines). The profiles of cells incubated with a Flag-tagged protein, which is unrelated to M-CSF, are also shown as a control (broken lines). B: TF-1 or TF-1-fms cells were seeded into 6-well culture plates at a density of 5×10^4 cells/ml in the absence or presence of the indicated concentrations of cytokines. TF-1 and TF-1-fms cells were cultured for 3 and 2 days, respectively. After the cultures, viable cells were enumerated. Error bars from triplicate assays are shown. These results are representative of two independent experiments. C: TF-1-fms cells were seeded at a density of 1×10^5 cells/ml, and cultured in the presence of M-CSF, TPA, or both. After culturing for 12 or 24 h, cells adhering to the dishes and non-adherent cells were enumerated. D–F: TF-1-fms cells were seeded at a density of 1×10^5 cells/ml, and cultured for 2 days in the presence of M-CSF (M-CSF), TPA (TPA), or both (M-CSF/TPA). D: The morphology of cells after culturing is shown. The cells cultured with M-CSF alone were photographed after a 5-fold dilution with media. E: The results of flow cytometric analyses of cells for forward and side scatters are shown. An equal number of cells were analyzed and the results are presented as counter plots. F: The phagocytic activity of cells was determined by the procedures described in the Materials and Methods (left panels). The percentage and mean fluorescence intensity (MFI) of cells in the region indicated by solid lines are shown. Alternatively, the cells were analyzed for the expression of CD204 by flow cytometry (right parts).

differentiation of TF-1-fms cells, using pharmacological inhibitors. As shown, PP2 (the inhibitor specific for Src kinases), PD98059 (the inhibitor specific for ERK kinase, MEK), and U0126 (another MEK inhibitor) significantly reduced the rate of M-CSF-mediated proliferation (Fig. 3A). The reduced proliferation rate correlated well with the increase in the percentage of PI-positive dead cells (Fig. 3A). Thus, we could not exclude the possibility that the inhibitory effect of these inhibitors on M-CSF-mediated proliferation reflected their cytotoxicity. Of importance, however, these inhibitors, in

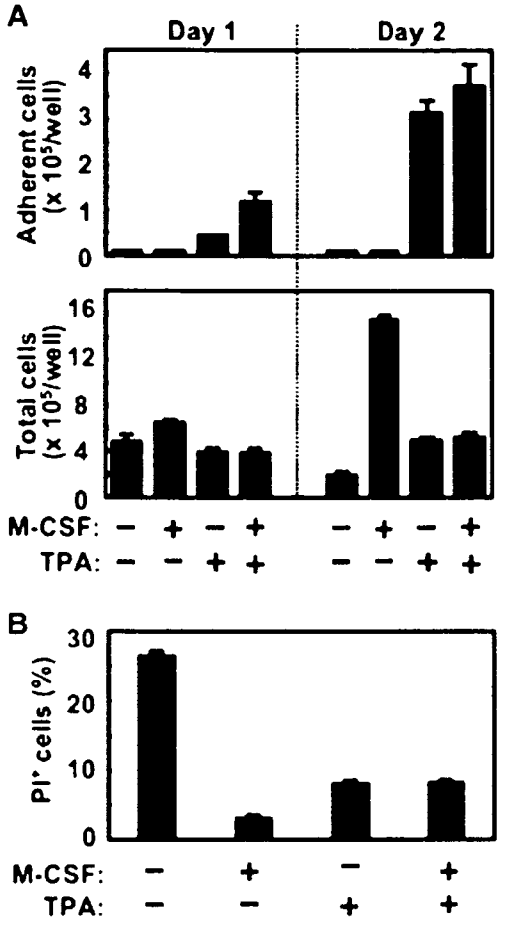

Fig. 2. A comparison of cell viability/death between the culture with TPA alone and that with M-CSF plus TPA. A and B: TF-1-fms cells were seeded into 6-well culture plates at a density of 1×10^5 cells/ml. Then, the cells were cultured in the absence of additives, or the presence of M-CSF, TPA, or both. A: After culturing for 1 or 2 days, cells adhering to the dishes (upper part) and all viable cells (lower part) were enumerated. B: After culturing for 2 days, the percentage of PI-positive dead cells in the wells was determined by flow cytometry. Error bars from triplicate assays are shown. These results are representative of two independent experiments.

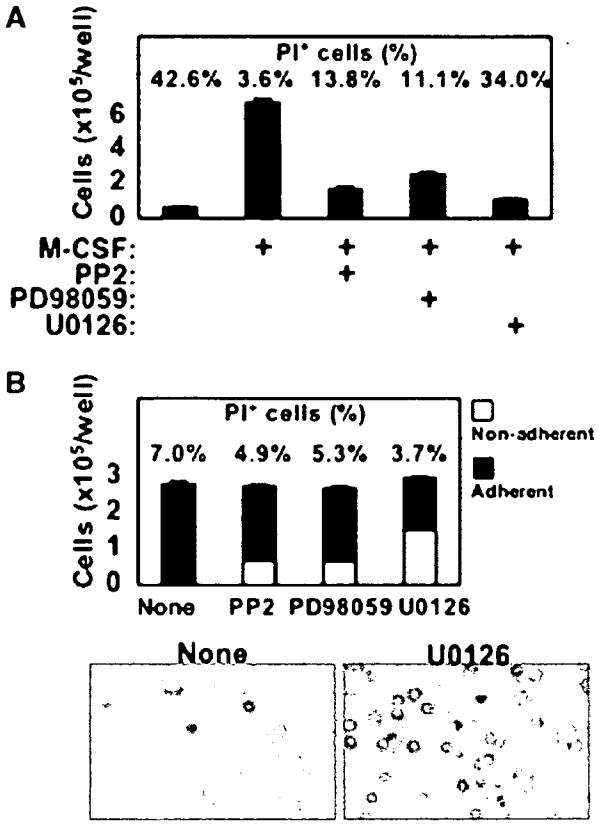

Fig. 3. Effects of pharmacological inhibitors on the proliferation and differentiation of TF-1-fms cells. A: TF-1-fms cells were seeded into 6-well culture plates at a density of 5×10^4 cells/ml in the absence or presence of the indicated inhibitors. M-CSF was added at a final concentration of 100 ng/ml. Both PP2 and U0126 were added at a final concentration of 10 μM. PD98059 was used at a final concentration of 50 μM. After culturing for 2 days, viable cells were enumerated. Error bars from triplicate assays are shown. Simultaneously, the percentage of PI-positive dead cells was determined by flow cytometry. These results are representative of two independent experiments. B: TF-1-fms cells were suspended at 1×10^5 cells/ml in medium containing M-CSF and TPA, and then cultured for 1 day in the absence or presence of the indicated inhibitors. The cells adhering to the dishes and non-adherent cells were enumerated. Error bars from triplicate assays are shown. Simultaneously, the percentage of PI-positive dead cells was determined by flow cytometry. These results are representative of two independent experiments. The morphology of cells after culturing is shown.

particular U0126, significantly inhibited the differentiation of TF-1-fms cells induced by M-CSF and TPA without increasing the percentage of PI-positive dead cells (Fig. 3B). These results indicated that the differentiation of TF-1-fms cells was dependent on the activation of ERK.

The level and duration of ERK activation in parental TF-1-fms cells

We next examined whether the increased and/or prolonged activation of ERK preceded the differentiation. We pretreated TF-1-fms cells with TPA or left them untreated, stimulated then with M-CSF or left them un-stimulated, and analyzed the activation of ERK by using an antibody specific for phosphorylated ERK (Fig. 4). Consistent with an earlier report (He et al., 1999), the treatment of TF-1-fms cells with TPA led to the ERK activation (Figs. 4A and B). Following M-CSF stimulation, a number of molecules were shown to be rapidly tyrosine-phosphorylated in both TPA-pretreated cells and untreated cells (Fig. 4A). The most prominent band at 150–160 kD, the tyrosine-phosphorylation level of which was reduced in the pretreated cells, seemed to be Fms (Suzu et al., 2005). The reduction of Fms phosphorylation in the pretreated cells was likely to be due to the reduced cell surface expression of Fms, because the pretreatment caused an increase in the intracellular form of Fms (gp130) and concomitant decrease in the cell surface form of Fms (gp150) (Fig. 4A), as seen in TPA-treated p388D1 macrophages (Wilhelmsen and van der Geer, 2004). Despite the reduced Fms phosphorylation, the level of ERK activation following M-CSF stimulation in TPA-pretreated cells was higher than that in untreated cells (Figs. 4A and B). Although the higher level of ERK activation following M-CSF stimulation seemed to be due to the high baseline level (Fig. 4A, the bar graph), the extent of the activation apparently correlated with the differentiation of TF-1-fms cells.

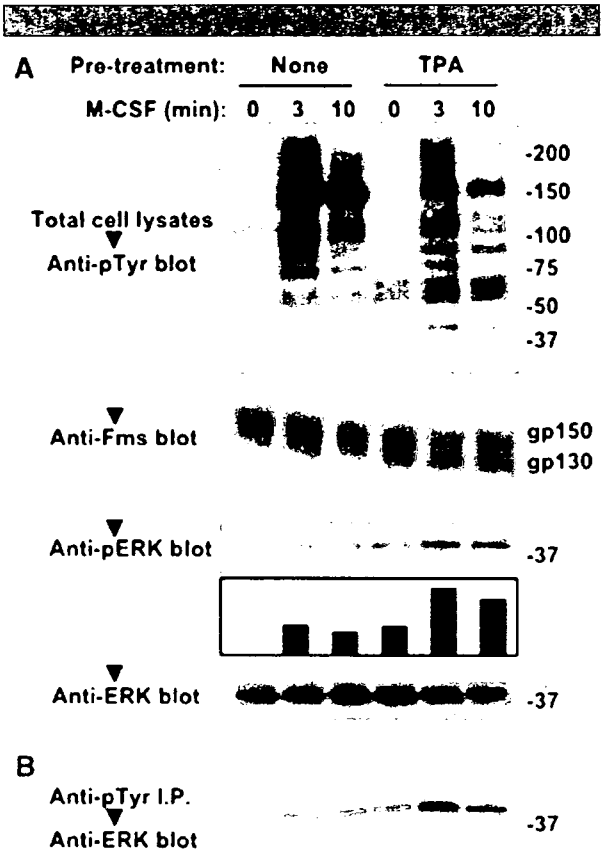

Fig. 4. The level of phosphorylation of ERK in TF-1-fms cells after pre-treatment with TPA and re-stimulation with M-CSF. TF-1-fms cells were deprived of M-CSF with or without TPA for 14 h and then re-stimulated with M-CSF for the indicated periods. A: Total cell lysates were analyzed with Western blotting using an antibody specific for phosphotyrosine (pTyr), Fms, phosphorylated ERK (pERK), or total ERK. The bottom blot was to show that comparable amounts of proteins were loaded in the upper blots. The relative intensities of bands on scanned gel images were quantified using the NIH Image software and the level of phosphorylated ERK normalized to the total amount of ERK is shown in the bar graph. B: The immunoprecipitates with anti-pTyr antibody were analyzed using anti-ERK antibody.

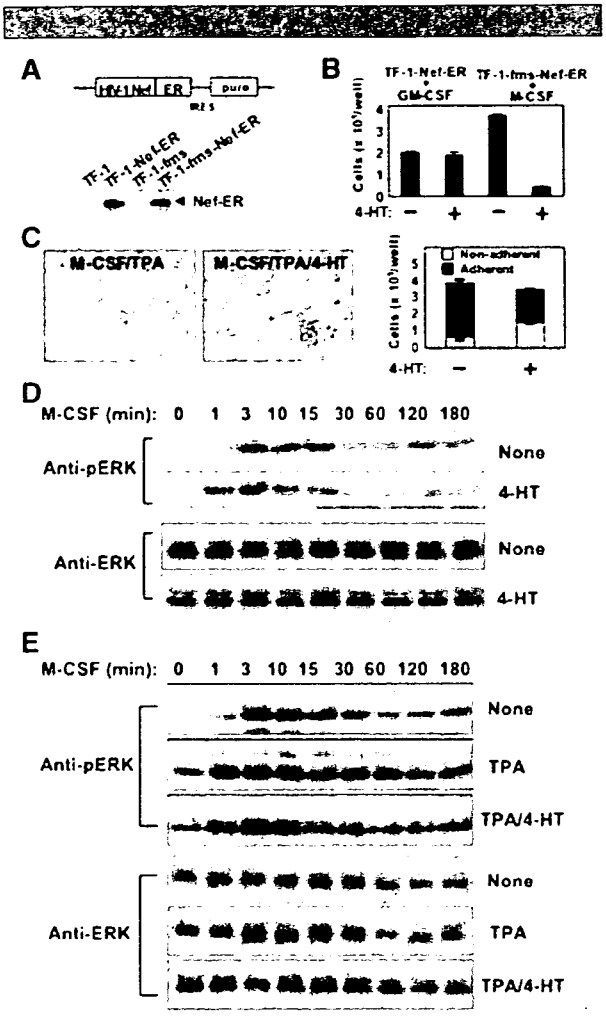

Fig. 5. Establishment of cells expressing the conditionally active Nef, proliferative/differentiative properties, and ERK activation. A: Schematic diagram of the Nef-ER-IRES-puro construct. ER, estrogen receptor hormone-binding domain; IRES, internal ribosomal entry sequence; puro, puromycin resistance gene. Total cell lysates from parental cells (TF-1 and TF-1-fms) or cells stably expressing Nef-ER (TF-1-Nef-ER and TF-1-fms-Nef-ER) were analyzed for the expression of Nef-ER by Western blotting with anti-Nef antibody. B: TF-1-Nef-ER cells were seeded at a density of 2×10^4 cells/ml and cultured in the presence of GM-CSF alone or GM-CSF plus 4-HT for 4 days. Similarly, TF-1-fms-Nef-ER cells were seeded at a density of 1×10^4 cells/ml and cultured in the presence of M-CSF alone or M-CSF plus 4-HT for 4 days. After the cultures, viable cells were enumerated. Error bars from triplicate assays are shown. These results are representative of two independent experiments. C: TF-1-fms-Nef-ER cells were suspended in medium containing M-CSF and TPA, and then cultured for 2 days in the absence (M-CSF/TPA) or the presence of 4-HT (M-CSF/TPA/4-HT). The cells adhering to the dishes and non-adherent cells were enumerated. Error bars from triplicate assays are shown. These results are representative of two independent experiments. D: TF-1-fms-Nef-ER cells were deprived of M-CSF for 14 h and then re-stimulated with M-CSF for the indicated periods. 4-HT was added to the culture at the beginning of the period of deprivation. Total cell lysates were prepared and analyzed by Western blotting using the antibody specific for phosphorylated ERK (upper part) or anti-total ERK antibody (lower part). E: As in D, TF-1-fms-Nef-ER cells were deprived of M-CSF for 14 h and then re-stimulated with M-CSF for the indicated periods. TPA or 4-HT was added to the culture at the beginning of the period of deprivation, as indicated. Total cell lysates were analyzed by Western blotting using the antibody specific for phosphorylated ERK (upper part) or anti-total ERK antibody (lower part). The result is representative of two independent experiments.

The proliferative/differentiative properties and the level/duration of ERK activation in TF-1-fms cells expressing conditionally active HIV-1 Nef

As mentioned above, we previously established TF-1-fms cells expressing the conditionally active HIV-1 Nef protein (the Nef-ER fusion protein) and showed that the activation of Nef by 4-HT caused the inhibition of the M-CSF-mediated proliferation of TF-1-fms cells (Figs. 5A and B; Suzu et al., 2005). By using the newly established TF-1 cells expressing the Nef-ER (Fig. 5A), we excluded the possibility that the inhibitory effect of Nef was due to non-specific cytotoxic activity of the viral protein: the activation of Nef did not affect GM-CSF-mediated proliferation of TF-1 cells (Fig. 5B). In this study, we found that Nef activation also caused the inhibition of the M-CSF/TPA-mediated differentiation of TF-1-fms cells (Fig. 5C). Consistent with its inhibitory effect on both M-CSF-mediated proliferation and M-CSF/TPA-mediated differentiation, Nef perturbed the patterns of ERK activation following the stimulation of TF-1-fms-Nef-ER cells with M-CSF (Figs. 5D and E). The untreated control cells

showed a biphasic ERK activation following M-CSF treatment. The early phase occurred between 1 and 3 min whereas the late phase started after 120 min (Fig. 5D). In contrast, the Nef-active cells whose proliferation rate was low showed an earlier but transient ERK activation following M-CSF stimulation (Fig. 5D). On the other hand, TPA-pretreated cells showed an increased and prolonged activation following M-CSF treatment when compared to the untreated control cells (Fig. 5E). Of importance, however, the Nef-active TPA-pretreated cells showed a transient ERK activation (Fig. 5E). These results suggested that the increased and prolonged activation of ERK correlated well with M-CSF/TPA-mediated differentiation, but not with M-CSF-mediated proliferation, of TF-1-fms cells.

Discussion

We established a new macrophage differentiation-inducing system that was dependent on M-CSF activity. TF-1-fms cells definitely switched their responsiveness to M-CSF from proliferation to differentiation in the presence of TPA (Fig. 1). Although the treatment with TPA alone triggered the macrophage differentiation of the cells, the presence of M-CSF enhanced the process: (1) the combination of both M-CSF and TPA caused more drastic morphological changes (Figs. 1C and D); (2) the culture in the presence of both M-CSF and TPA contained more adherent cells than that in the presence of TPA alone (Fig. 2A, upper part); (3) the phagocytic activity and the expression of CD204 were significantly higher in cells treated with M-CSF and TPA than those treated with TPA alone (Fig. 1E). The macrophage differentiation by M-CSF and TPA did not reflect the survival-enhancing/anti-apoptotic function of M-CSF (Fig. 2A, lower part and B).

The experiments with the pharmacological inhibitor U0126 showed that M-CSF/TPA-mediated differentiation of TF-1-fms was dependent on ERK activation (Fig. 3B). That the Src inhibitor PP2 was also a potent inhibitor of the responses (Fig. 3B) might reflect the finding that the activation of ERK by M-CSF was in part dependent on the activity of Src kinases (Cheng et al., 1999; McMahon et al., 2001). However, the involvement of the increased and/or prolonged ERK activation in M-CSF-mediated differentiation is somewhat controversial. Unlike murine M1 cells expressing wild-type Fms, the cells expressing Y559F mutant Fms showed an impaired differentiative response to M-CSF and a reduced level of ERK activation (McMahon et al., 2001). The enforced expression of a scaffolding protein, Gab2, in wild-type Fms-expressing FDC-P1 cells resulted in an acceleration of the differentiation process and increased ERK activation (Liu et al., 2001). In contrast, the enforced expression of an adapter protein, Mona, in wild-type Fms-expressing FDC-P1 cells resulted in increased and prolonged ERK activation, but not an acceleration of M-CSF-mediated differentiation (Bourgin et al., 2000). Moreover, 32D myeloid cells expressing the Y559F mutant Fms showed a "hyper-proliferative" response to M-CSF and prolonged ERK activation (Rohde et al., 2004). Our studies with parental and Nef-expressing TF-1-fms cells (Figs. 4 and 5) supported the former idea that increased and prolonged ERK activation led to M-CSF-mediated macrophage differentiation, but not to cell proliferation. The TPA-pretreated parental TF-1-fms cells (differentiative) showed increased and prolonged ERK activation following M-CSF stimulation (Fig. 4). In contrast, the Nef-active TPA-pretreated TF-1-fms (un-differentiative) showed transient ERK activation (Figs. 5C and E). The pharmacological agent GF109203X, a potent inhibitor of the expression of MAPK phosphatase-1 (Valledor et al., 1999), caused TF-1-fms cells to differentiate in the presence of M-CSF and the cells pretreated with GF109203X showed a sustained ERK activation following M-CSF treatment (data not shown), further supporting the idea.

The molecular mechanisms whereby Nef inhibited the M-CSF-mediated proliferation and M-CSF/TPA-mediated differentiation of TF-1-fms cells remained to be elucidated. In TF-1-fms cells, Nef activation induced the activation of Hck and its constitutive association with Fms (Suzu et al., 2005). The unphysiological behavior of Hck might explain the inhibitory effect of Nef on the responsiveness to M-CSF. Yet, under the proliferation-inducing conditions (TPA-free), the activation of Nef resulted in an earlier ERK activation (Fig. 5D). This might be explained by the finding that Nef induced ERK activation in $CD4^+$ T cells (Schrager et al., 2002) and podocytes (He et al., 2004) in a Src-dependent manner. Further experiments are required to understand the molecular mechanisms whereby Nef rapidly terminated ERK activation in the presence of TPA (Fig. 5E). In summary, we showed that M-CSF-mediated macrophage differentiation, but not proliferation was correlated with increased and prolonged ERK activation, by using a newly established macrophage-inducing system. The culture system with Nef-expressing TF-1-fms cells provides a useful tool for determining the temporal regulatory mechanism of ERK activation and its contribution to M-CSF-mediated proliferation/differentiation.

Acknowledgments

We thank Ranko Shimamura and Yuka Endo for technical and secretarial assistance, respectively.

Literature Cited

Bourette RP, Rohrschneider LR. 2000. Early events in M-CSF receptor signaling. Growth Factors 17:155–166.

Bourette RP, Myles GM, Carlberg K, Chen AR, Rohrschneider LR. 1995. Uncoupling of the proliferation and differentiation signals mediated by the murine macrophage colony-stimulating factor receptor expressed in myeloid FDCP-1 cells. Cell Growth Diff 6:631–645.

Bourgin C, Bourette R, Mouchiroud G, Arnaud S. 2000. Expression of Mona (monocytic adapter) in myeloid progenitor cells results in increased and prolonged MAP kinase activation upon macrophage colony-stimulating factor stimulation. FEBS Lett 480:113–117.

Cheng M, Wang D, Roussel MF. 1999. Expression of c-Myc in response to colony-stimulating factor-1 requires mitogen-activated protein kinase kinase-1. J Biol Chem 274:6553–6558.

Fackler OT, Baur AS. 2002. Live and let die: Nef functions beyond HIV replication. Immunity 16:493–497.

Gredinger E, Gerber AN, Tamir Y, Tapscott SJ, Bengal E. 1998. Mitogen-activated protein kinase pathway is involved in the differentiation of muscle cells. J Biol Chem 273:19436–10444.

Hashimoto S, Suzuki T, Dong HY, Yamazaki N, Matsushima K. 1999. Serial analysis of gene expression in human monocytes and macrophages. Blood 94:837–844.

He H, Wang X, Gorospe M, Holbrook NJ, Trush MA. 1999. Phorbol ester-induced mononuclear cell differentiation is blocked by the mitogen-activated protein kinase kinase (MEK) inhibitor PD98059. Cell Growth Diff 10:307–315.

He JC, Husain M, Sunamoto M, D'Agati VD, Klotman ME, Iyengar R, Klotman PE. 2004. Nef stimulates proliferation of glomerular podocytes through activation of Src-dependent Stat3 and MAPK1, 2 pathways. J Clin Invest 114:643–651.

Kitamura T, Tange T, Terasawa T, Chiba S, Kuwaki T, Miyagawa K, Piao YF, Miyazono K, Urabe A, Takaku F. 1989. Establishment and characterization of a unique human cell line that proliferates dependently on GM-CSF, IL-3, or erythropoietin. J Cell Physiol 140:323–334.

Liu Y, Jenkins B, Shin JL, Rohrschneider LR. 2001. Scaffolding Gab2 mediates differentiation signaling downstream of Fms receptor tyrosine kinase. Mol Cell Biol 21:3047–3056.

Marks DC, Csar XF, Wilson NJ, Novak U, Ward AC, Kanagasundarum V, Hoffmann BW, Hamilton JA. 1999. Expression of a Y559F mutant CSF-1 receptor in M1 myeloid cells: a role of Src kinases in CSF-1 receptor-mediated differentiation. Mol Cell Biol Res Commun 1:144–152.

Marshall CJ. 1995. Specificity of receptor tyrosine kinase signaling: transient versus sustained extracellular signal-regulated kinase activation. Cell 80:179–185.

McMahon K-E, Wilson NJ, Marks DC, Beecroft TL, Whitty GA, Hamilton JA, Csar XF. 2001. Colony-stimulating factor-1 (CSF-1) receptor-mediated macrophage differentiation in myeloid cells: a role for tyrosine 559-dependent protein phosphatase 2A (PP2A) activity. Biochem J 358:431–436.

Melemed AS, Ryder JW, Vik TA. 1997. Activation of the mitogen-activated protein kinase pathway is involved in and sufficient for megakaryocytic differentiation of CMK cells. Blood 90:3462–3470.

Moarefi I, LaFevre-Bernt M, Sicheri F, Huse M, Lee C-H, Kuriyan J, Miller WT. 1997. Activation of the Src-family tyrosine kinase Hck by SH3 domain replacement. Nature 385:650–653.

Okada S, Zhang H, Hatano M, Tokuhisa T. 1998. A physiological role of Bcl-$_{xL}$ induced in activated macrophages. J Immunol 160:2590–2596.

Peterlin BM, Trono D. 2003. Hide, shield and strike back: how HIV-infected cells avoid immune eradication. Nat Rev Immunol 3:97–107.

Qiao X, He B, Chiu A, Knowles DM, Chadburn A, Cerutti A. 2006. Human immunodeficiency virus 1 Nef suppresses CD40-dependent immunoglobulin class switching in bystander B cells. Nat Immunol 7:302–310.

Racke FK, Lewandowska K, Goueli S, Goldfarb AN. 1997. Sustained activation of the extracellular signal-regulated kinase/mitogen-activated protein kinase pathway is required for megakaryocytic differentiation of K562 cells. J Biol Chem 272:23366–23370.

Rohde CM, Schrum J, Lee AW-M. 2004. A juxtamembrane tyrosine in the colony stimulating factor-1 receptor regulates ligand-induced Src association, receptor kinase function, and down-regulation. J Biol Chem 279:43448–43461.

Roth P, Stanley ER. 1992. The biology of CSF-1 and its receptor. Curr Top Microbiol Immunol 181:141–167.

Roussel MF, Shurtleff SA, Downing JR, Sherr CJ. 1990. A point mutation at tyrosine-809 in the human colony-stimulating factor 1 receptor impairs mitogenesis without abrogating tyrosine kinase activity, association with phosphatidylinositol 3-kinase, or induction of *c-fos* and *junB* genes. Proc Natl Acad Sci USA 87:6738–6742.

Saksela K, Cheng G, Baltimore D. 1995. Proline-rich (PxxP) motifs in HIV-1 Nef bind to SH3 domains of a subset of Src kinases and are required for the enhanced growth of Nef^+ viruses but not for down-regulation of CD4. EMBO J 14:484–491.

Schrager JA, Der Minassian V, Marsh JW. 2002. HIV Nef increases T cell ERK MAP kinase activity. J Biol Chem 277:6137–6142.

Sherr CJ, Rettenmier CW, Sacca R, Roussel MF, Look AT, Stanley ER. 1985. The *c-fms* proto-oncogene product is related to the receptor for the mononuclear phagocyte growth factor, CSF-1. Cell 41:665–676.

Suzu S, Kimura F, Ota J, Motoyoshi K, Itoh T, Mishima Y, Yamada M, Shimamura S. 1997. Biologic activity of proteoglycan macrophage colony-stimulating factor. J Immunol 159:1860–1867.

Suzu S, Tanaka-Douzono M, Nomaguchi K, Yamada M, Hayasawa H, Kimura F, Motoyoshi K. 2000. $p56^{dok-2}$ as a cytokine-inducible inhibitor of cell proliferation and signal transduction. EMBO J 19:5114–5122.

Suzu S, Harada H, Matsumoto T, Okada S. 2005. HIV-1 Nef interferes with M-CSF receptor signaling through Hck activation and inhibits M-CSF bioactivities. Blood 105:3230–3237.

Tomokiyo R, Jinnouchi K, Honda M, Wada Y, Hanada N, Hiraoka T, Suzuki H, Kodama T, Takahashi K, Takeya M. 2002. Production, characterization, and interspecies reactivities of monoclonal antibodies against human class A macrophage scavenger receptors. Atherosclerosis 161:123–132.

Valledor AF, Xaus J, Marques L, Celeda A. 1999. Macrophage colony-stimulating factor induces the expression of mitogen-activated protein kinase phosphatase-1 through a protein kinase C-dependent pathway. J Immunol 163:2452–2462.

Valledor AF, Comalada M, Xaus J, Celeda A. 2000. The differential time-course of extracellular-regulated kinase activity correlates with the macrophage response toward proliferation or activation. J Biol Chem 275:7403–7409.

van der Geer P, Hunter T. 1993. Mutation of Tyr697, a GRB2-binding site, and Tyr721, a PI 3-kinase binding site, abrogates signal transduction by the murine CSF-1 receptor expressed in Rat-2 fibroblasts. EMBO J 12:5161–5172.

Walk SF, Alexander M, Maier B, Hammarskjold M-L, Rekosh DM, Ravichandran KS. 2001. Design and use of an inducibly activated immunodeficiency virus type 1 Nef to study immune modulation. J Virol 75:834–843.

Wilhelmsen K, van der Geer P. 2004. Phorbol 12-myristate 13-acetate-induced release of the colony-stimulating factor 1 receptor cytoplasmic domain into the cytosol involves two separate cleavage events. Mol Cell Biol 24:454–464.

Immunity to infection

Proliferative activation up-regulates expression of CD4 and HIV-1 co-receptors on NK cells and induces their infection with HIV-1

Hideki Harada[1,2], Yumi Goto[1], Tadao Ohno[3], Shinya Suzu[1] and Seiji Okada[1]

[1] Division of Hematopoiesis, Center for AIDS Research, Kumamoto University, Kumamoto, Japan
[2] Japanese Foundation for AIDS Prevention, Tokyo, Japan
[3] Cell-Medicine Inc., Tsukuba, Ibaraki, Japan

NK cells play important roles in immune surveillance against malignancy and virus-infected cells. NK cell functions are affected in patients infected with HIV-1; however, whether there is direct interaction between NK cells and HIV-1 remains controversial. In this study the expression of CD4, an important receptor for HIV-1, was up-regulated on NK cells co-cultured with an NK cell-selective stimulating cell line, HFWT, and rIL-2. Although the level of CD4 was lower on NK cells than on $CD4^+$ T cells, expression of the HIV-1 co-receptor CCR5 was clearly up-regulated on $CD4^+$ NK cells. $CD4^+$ NK cells expressed higher levels of HLA-DR and CD25 than $CD4^-$ NK cells, suggesting that they were highly activated. Cell-free HIV-1 could not infect the NK cells, but NK cells were infected when co-cultured with HIV-1-infected T cells. Using this co-culture system, we can better understand how HIV-1 infects NK cells and how NK cell functions are affected in AIDS.

Received 18/2/07
Revised 18/4/07
Accepted 13/6/07

[DOI 10.1002/eji.200737217]

Key words: Cellular activation · HIV · Natural killer cells

Introduction

NK cells play critical roles in immune surveillance without deliberate prior sensitization or restriction by MHC. Human NK cells can be divided into $CD56^{dim}CD16^+$ and $CD56^{bright}CD16^-$ populations: the former are highly cytotoxic, while the latter produce large amounts of cytokines. The cytotoxicity of NK cells is regulated by various activating and inhibitory receptors at the cell surface [1]. In AIDS patients, numbers and function of NK cells are altered. For example, in viremic HIV-1 patients, expression levels of inhibitory receptors are increased. Expression levels of activation receptors, antibody-dependent cellular cytotoxicity (ADCC), production of anti-HIV-1 CC-chemokines, and maturation of DC by NK cells are all affected by HIV infection [2]. However, because CD4, a key receptor for HIV-1 infection, is generally not found on peripheral blood (PB) NK cells, it is difficult to clarify the direct interaction between HIV-1 and NK cells. At present, HIV-1 infection of NK cells remains a controversial issue. Valentin *et al.* demonstrated that HIV-1-infected NK cells constitute a long-living viral reservoir in AIDS patients [3]. In contrast, Mavilio *et al.* reported that HIV-1 proviral DNA was not detected in freshly isolated blood NK cells from viremic patients, although the phenotype and function of the NK cells were dramatically changed [4]. Therefore, it is thought that one approach to revealing NK cell abnormality in AIDS is to find evidence of HIV-1 infection of NK cells.

CD4 is generally expressed on helper T cells and monocytes/macrophages as well as on subsets of leukocytes such as dendritic cells [5], γδ T cells [6],

Correspondence: Seiji Okada, Division of Hematopoiesis, Center for AIDS Research, Kumamoto University, 2-2-1 Honjo, Kumamoto 860–0811, Japan
Fax: +81-96-373-6523
e-mail: okadas@gpo.kumamoto-u.ac.jp

Abbreviations: APC: allophycocyanin · **CB:** cord blood · **CBMC:** cord blood mononuclear cell · **PB:** peripheral blood